Journal of Civil Structural Health Monitoring
https://doi.org/10.1007/s13349-024-00824-7

ORIGINAL PAPER

Seismic response and ambient vibrations of a Mediaeval Tower in the Mugello area (Italy)

R. M. Azzara[1] · V. Cardinali[2] · M. Girardi[3] · C. Padovani[3] · D. Pellegrini[3] · M. Tanganelli[2]

Received: 6 April 2024 / Accepted: 22 June 2024

Abstract

This paper describes the experimental campaigns on the Tower of the Palazzo dei Vicari in Scarperia, a village in the Mugello area (Tuscany) exposed to high seismic hazards. The first campaign was carried out from December 2019 to January 2020, and the Tower underwent the so-called Mugello seismic sequence, which featured an M 4.5 earthquake. Other ambient vibration tests were repeated in June 2021 and September 2023 when another seismic sequence struck the area near Scarperia. These tests aimed to characterise the Tower's dynamic behaviour under ambient and seismic excitations and check the response of the Tower over time. The experimental results were then used to calibrate a finite-element model of the Tower and estimate its seismic vulnerability. Several numerical simulations were conducted on the calibrated model using the NOSA-ITACA code for nonlinear structural analysis of masonry buildings. The dynamic behaviour of the Tower subjected to a seismic sequence recorded in 2023 by a seismic station at the base was investigated by comparing the velocities recorded along the Tower's height with their numerical counterparts. Furthermore, several pushover analyses were conducted to investigate the collapse of the Tower as the load's distribution and direction varied.

Keywords Historical buildings · Experimental seismic campaign · Dynamic identification · Finite-element model updating · Nonlinear dynamics

1 Introduction

A high level of seismic hazard characterises Italy all over the country. The tectonic theory identifies the main reason for the seismic activity characterising the Mediterranean area in the collision between the African and European plates. The distribution of seismicity in Italy follows the contour of the Apennines, the rocky backbone of the peninsula. In the past 20 years, the areas placed in the Northern and Central Apennines have been affected by strong to moderate earthquakes: from the 1997 Umbria-Marche M 5.6 and 5.8 earthquakes [18] up to the 2016 Amatrice–Norcia earthquakes, M 6.2 [41] and M 6.5 [56]. Other lower magnitude earthquakes may be added to this list: the 2002, M 5.7 San Giuliano event [18] and the 2012 M 5.8 and 5.9 Emilia earthquakes [57]. These events produced damages for many billions of Euros and hundreds of fatalities.

Despite the not-so-high magnitude of the recorded earthquakes in the recent past, the seismic risk of the entire peninsula is significantly high due to the combined contribution of hazard, vulnerability, and exposure. Ground shaking amplification related to site effects may locally increase

✉ D. Pellegrini
daniele.pellegrini@isti.cnr.it

R. M. Azzara
riccardo.azzara@ingv.it

V. Cardinali
vieri.cardinali@unifi.it

M. Girardi
maria.girardi@isti.cnr.it

C. Padovani
cristina.padovani@isti.cnr.it

M. Tanganelli
marco.tanganelli@unifi.it

[1] Osservatorio Sismologico di Arezzo, Istituto Nazionale di Geofisica e Vulcanologia (INGV), Arezzo, Italy

[2] Dipartimento di Architettura (DiDA), Università degli Studi di Firenze, Florence, Italy

[3] Istituto di Scienza e Tecnologie dell'Informazione "A. Faedo" (ISTI-CNR), Pisa, Italy

Published online: 01 July 2024

the magnitude and the risk; moreover, regarding cultural and architectural heritage, the relevant vulnerability of the urban stock combines with a not always quantifiable value of exposure.

In this regard, since a few years ago, structural health monitoring (SHM) has been established as an essential tool for assessing the structural performances of monumental buildings.

In line with the widespread approach of Operational Modal Analysis (OMA) [15], data recorded by the velocimeters and accelerometers installed on the building in operating conditions are processed using specific numerical procedures to determine its dynamic properties (frequencies, damping ratios and mode shapes). Tracking the variation of frequencies over time, assessing the response of a building to the environmental excitations of natural and anthropic origin (earthquakes, wind, traffic, machinery, and moving crowds) and analysing changes and anomalies in its dynamic behaviour are essential ingredients of SHM.

Long-term monitoring protocols allow the measurement of the buildings' response to several external excitations, including seismic actions; combined with finite element (FE) codes, such protocols can help evaluate the buildings' static and seismic vulnerability. Despite that, the scientific literature reports on very few cases of long-term monitoring of ancient buildings. This fact is in large part attributable to the cost of the high-sensitivity instrumentation needed for monitoring the vibrations of massive masonry buildings in operational conditions.

Examples of long-term monitoring of ancient masonry structures are shown in Refs. [43, 52] concerning some monumental structures in Portugal. Gentile et al. [32] report on the dynamic monitoring of an ancient tower in Mantua, García-Macías and Ubertini [30] describe the results of long-term monitoring conducted on a bell tower in Perugia, Gentile et al. [31] present the results of a permanent dynamic monitoring system in the Milan Cathedral, and Di Giulio et al. [24] provide information on the monitoring of a monumental church damaged during the 2009 earthquake of L'Aquila. Also, the authors of the present paper contributed to several long-term dynamic monitoring campaigns, such as Baraccani et al. [11] on the structural health monitoring of the Two Towers in Bologna, Azzara et al. [5, 6] on the dynamic monitoring campaign on some historical towers in Lucca, Barsocchi et al. [12] on the dynamic monitoring of the Old Fortress in Livorno via MEMS technology, and recently [8] on the continuous monitoring of the Arnolfo Tower in Florence.

Many of the systems above were able to measure low-amplitude earthquakes and, in some cases [32, 62], to reveal the onset of damage in the monitored structures, highlighted by an abrupt permanent change in the natural frequencies. The authors of the paper [2] recorded the effects of low-amplitude seismic events on the Basilica of Santa Maria di Collemaggio after the large restoration operations that involved the church following the 2009 L'Aquila earthquake. They found a drop in the church's natural frequencies during the earthquakes, and it disappeared after the events, proving the absence of minor structural damage due to low-to-moderate earthquakes.

Several recent papers [7, 23, 27, 51, 55, 58, 65] adopted a combined experimental and numerical approach for evaluating the dynamic behaviour of masonry towers. In Ref. [55], ambient vibration tests (AVT) were used to calibrate an FE model of the Giralda Tower in Seville, which was subsequently used to analyse the seismic behaviour of the structure via nonlinear static analysis. In Ref. [65], the seismic damage on historical masonry towers was assessed by integrating FE numerical simulations and experimental data obtained using shaking table tests and adopting frequency changes as damage indicators. In Ref. [27], the seismic performance of the Bayburt clock tower in Turkey, before and after restoration operations, is assessed using an FE model calibrated via AVT and subjected to selected earthquake accelerograms. In Ref. [23], the seismic response of the Saint Lawrence Cathedral's bell tower in Genoa is predicted by integrating AVTs with simplified numerical models, focusing on the safety evaluations of the pinnacles.

Papers [51] and [58] mainly focus on experimental-based FE model updating. The former is devoted to comparing Bayesian and deterministic FE model updating of the San Felice sul Panaro fortress, and the latter presents an FE model calibration of the Clock Tower of Rotella in central Italy obtained via a combined approach based on sensitivity analysis and genetic algorithms for global minimisation. Finally, the authors of the paper [9] present the experimental and numerical investigations conducted on a carillon tower in Italy aimed at assessing the swinging bells' effects on the structure's dynamic behaviour.

The nonlinear static pushover analysis approach has been adopted in several papers to evaluate the response of masonry towers under seismic loading. In Ref. [50], the suitability of applying pushover analysis to predict the dynamic response of free-standing slender masonry towers has been investigated by considering different geometrical and mechanical properties, several load distributions and modelling the towers via beam elements made of a masonry-like material. In Ref. [1], pushover analyses were conducted to investigate the towers' collapse that occurred on the occasion of the 2012 Emilia Romagna seismic sequences and assess the structural performance of virtual rehabilitation interventions simulated on the numerical models of the towers after the earthquake. The pushover analyses in Ref. [63] allowed the seismic response assessment of eight masonry towers in Italy by modelling the constituent material via a damage plasticity approach. In Ref.[13], a numerical procedure is

proposed to perform force-driven pushover analyses with displacement control by considering geometrical and material nonlinearities. The procedure was applied to the Gabbia Tower in Mantova. Other applications of the pushover approach are described in Ref. [29], focused on the Santa Maria a Vico bell tower (Italy) and in Ref. [22], where the seismic performance of the church of San Juan Bautista—Inca temple of Huaytara (Peru) is investigated.

The present paper focuses on the dynamic monitoring of the Tower of the Palazzo dei Vicari in the historic centre of Scarperia, a village in the Mugello area (Tuscany) exposed to high seismic hazards. The historic centre of Scarperia has been recently subject of a vulnerability survey carried by the Architecture Department (DIDA) of the University of Florence which has allowed obtaining geometrical and structural information on the different building aggregates [17]. The Tower of Palazzo dei Vicari was the subject of three experimental campaigns. The first was carried out from December 2019 to January 2020 on the occasion of the so-called Mugello seismic sequence, the most relevant event of which was an M 4.5 earthquake. Other measurements were repeated in June 2021, during which no seismic sequences were recorded on the tower, and in September 2023 when another seismic sequence struck the area near Scarperia. These tests aimed to characterise the Tower's dynamic behaviour under ambient and seismic excitations and check the response of the Tower over time. The experimental results are presented and discussed in the paper and the vibrations of the Tower recorded during the seismic sequences of December 2019 are examined. Finally, the experimental results are adopted to calibrate an FE model of the Tower. Several numerical simulations were conducted on the calibrated model using the FE code NOSA-ITACA developed at ISTI-CNR [34]. The dynamic behaviour of the Tower subjected to a seismic sequence recorded on 21 September 2023 by the station placed at the base has been investigated by comparing the velocities recorded by a station on the Tower's top with their numerical counterparts. Furthermore, several pushover analyses were conducted to investigate the collapse of the Tower as the load's distribution and direction varied.

2 The experimental campaigns on the Tower of Palazzo dei Vicari

The Mugello, a region located 20 km far from Florence (Tuscany), is a hilly area exposed to a high seismic hazard. It divides the Florentine Valley from the Apennines mountains and is characterised by small, isolated urban centres. From the tectonic point of view, the area's seismic activity is related to the Etrurian System Fault, which is localised from Umbria to Tuscany and includes the Garfagnana and Lunigiana regions [14, 40]. The last strong seismic event

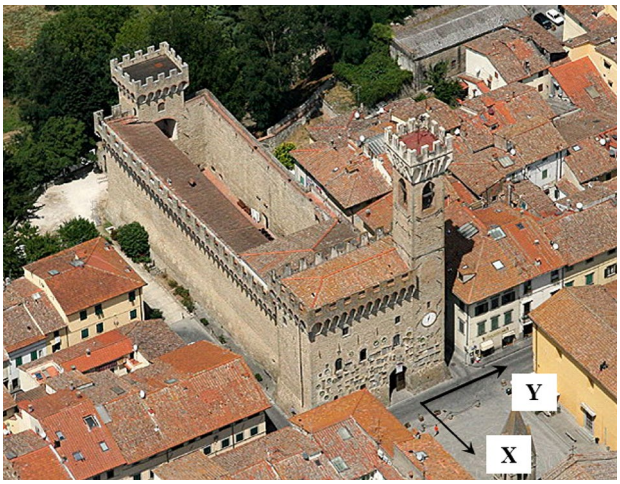

Fig. 1 The historic centre of Scarperia, Tuscany: aerial view

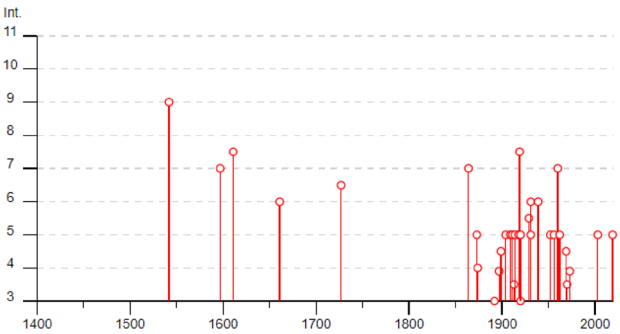

Fig. 2 Timeline of the seismicity in Scarperia from 1440 (DMBI15, the Italian Macro-seism Database), the intensity is expressed in MCS scale

occurred in the area about one hundred years ago, on 29 June 1919, with magnitude M 6.3 [37, 42]. The event destroyed the city of Vicchio, and many centres of the area suffered heavy damage [3].

The historic centre of Scarperia (Fig. 1), a city founded over a hill of the Mugello area during the Mediaeval period by the Republic of Florence, is the target of this study. In the past, the city was struck by many earthquakes. Figure 2, extracted from DBM15, the Italian Macro-seismic Database [38], shows the intensity of the seismic events in Scarperia from 1400 to now.

On 9 December 2019 02:37 UTC, an M 4.5 earthquake occurred in the area. The event, preceded by other earthquakes since 8 December, was located by the National Seismic Network of the Italian National Institute of Geophysics and Volcanology (INGV) at about 5 km from Scarperia, at a depth of 9 km (Fig. 3). The seismic sequence started on 8 December and lasted until mid-January 2020, producing about 300 events whose magnitude ranged from 0.5 to 4.5. Among these events, only 11 exceeded magnitude 3. The

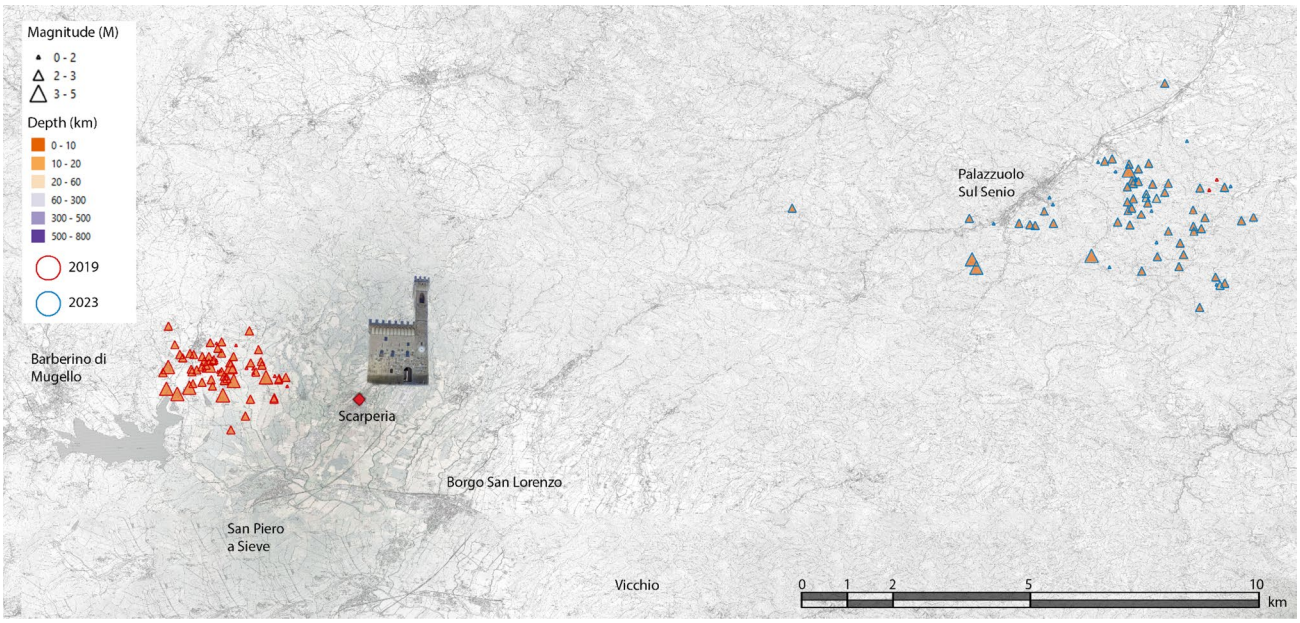

Fig. 3 Localisation of the main recent seismic events in the surroundings of Palazzo dei Vicari, Scarperia. The position of Palazzo dei Vicari is reported in the centre of Scarperia; the red triangles indicate the epicentral positions of the 2019 seismic sequence, the blue ones the sequence of 2023

latest relevant seismic sequence in the area dates back to September 2023; the most energetic event of this sequence was an M 4.9 earthquake that struck the city of Marradi, near Scarperia, on 18 September (Fig. 3).

During the 2019 seismic sequence, the Tower of the Palazzo dei Vicari (Fig. 4) in the historic centre of Scarperia (Fig. 1) was the subject of a monitoring campaign carried out by the Architecture Department (DIDA) of the University of Florence and the Seismological Observatory of Arezzo of INGV. On 9 December (after the M 4.5 mainshock), two seismic stations were installed in the Tower, a slender mediaeval structure connected to the main palace. Although the most energetic portion of the seismic sequence ran out in the first hours after the mainshock, when the seismic stations were not yet installed on the Tower, it was possible to record 22 earthquakes with a magnitude between 1.8 and 3.1, thus evaluating the Tower's structural response under seismic actions. In June 2021, a further experimental campaign was performed to improve the Tower's dynamic characterisation. INGV and the Institute of Information Science and Technologies "A. Faedo" (ISTI-CNR) installed seven seismometers at different heights along the structure. Finally, a last campaign was conducted in September 2023, during the most recent seismic sequence. The mainshock was recorded at 03:10 (UTC Italian time) on 18 September 2023, with an epicentre 3 km southwest of Marradi (M 4.9, depth 8.4 km) and it was preceded at 02:38 by an earthquake of intensity M 3.4. In the following hours, three velocimeters were installed at different heights, allowing the recording of part of the seismic sequence.

Fig. 4 View of the Palazzo dei Vicari and its Tower

2.1 The Tower of Palazzo dei Vicari

Palazzo dei Vicari (Fig. 4) represents the most iconic landmark in the city of Scarperia. The Florentine Republic built the city during mediaeval times by adopting a regular scheme [17]. The historical centre follows the Roman scheme of *cardo* and *decumanus*; the main front of Palazzo dei Vicari faces the main square of the city, located at the intersection within the principal road axes. The first documents on Palazzo dei Vicari date back to 1306, with the approval of the construction of Castle Santa Barbara, the original name of the Palace. The building shows its Florentine origins in the architectural concept and the exterior decorations, which emulate Palazzo Vecchio in Florence on a smaller scale [16]. The castle's construction started in 1355, and the significant dimensions of its inner courtyard (Fig. 5) suggest that it was intended to house the city's entire population in case of conflict. In the XV century, the city's administrative functions went to the *Vicario*, who lived in the Palace and gave the name to the structure. Palazzo dei Vicari became the administrative district of a large territory comprehending a significant part of the Mugello area. The civic value of the building is still visible in the decorative elements which cover its main façade (coats of arms). The Tower of the Palace is in the Northern corner of the building.

Specific documentation regarding the Tower is not available. The clock, designed by Filippo Brunelleschi, represents the most traced element. The original mechanism has been removed from the Tower, and the clock visible today on the façade is only a decoration.

Fig. 5 The inner courtyard of Palazzo dei Vicari, view from the entrance to the Palace

The Tower is about 40 m high and characterised by a squared transverse section with the external walls enlarging their base through buttress elements (Fig. 6). The Tower is adjacent to Palazzo dei Vicari and connected to the building's structure through two inner floors (vaults and wooden slabs) and a roof structure. At the top of the slender architecture, the bell chamber houses the historical bells, which are no longer allowed to oscillate at the change of the hours. Finally, the top of the Tower is made of a wooden roof and castle merlons. The building-tower complex shows the consequences of the high seismicity of the Mugello territory, and several steel tie rods embrace the masonry structures of the Palace. Multiple layers of tie rods strengthen the Tower at different heights, and the different finishes of the bolted end plates indicate a continuous insertion of the reinforcements over the centuries.

The dynamic monitoring of the Tower was conducted using tri-axial velocimeters (SS45 and SS20 produced by SARA Electronic Instruments, Perugia), each equipped with a digital acquisition system SL06 (24-bit digitiser). Figure 6 shows the geometry of the Tower and the sensor layouts adopted in the three monitoring campaigns conducted in 2019, 2021 and 2023. The seismic stations were installed at different heights, from the base to the bell chamber (see Fig. 6) and synchronised through a GPS connection. Each instrument's x and y axes were aligned with the X and Y axes shown in Fig. 1.

2.2 First experimental campaign (December 2019–January 2020)

Two seismic stations, one at the base and the other at the top, were installed on the Tower on 9 December 2019 and run until 4 January 2020, with a sampling frequency of 200 Hz (Fig. 6). Data recorded by the station at the base is available only from 16 December to 4 January. According to the information provided by the National Earthquake Observatory (ONT) of the INGV, the seismic sequence produced about 290 events (M from 0.5 to 4.5) from 8 December 2019 until 26 December (sporadic weaker events also occurred in the first ten days of January). Only 66 earthquakes exhibit a magnitude greater than 2.0. Fifty-four of them happened during the first 2 days of seismic activity, before the complete installation of all the instruments. The strongest event of the sequence was an M 4.5 earthquake on 9 December, located about 5 km from Scarperia.

Among all the earthquakes recorded during the monitoring period, 22 events ranging between M 1.8 and 3.1 have been selected and shown in Table 1. The most energetic

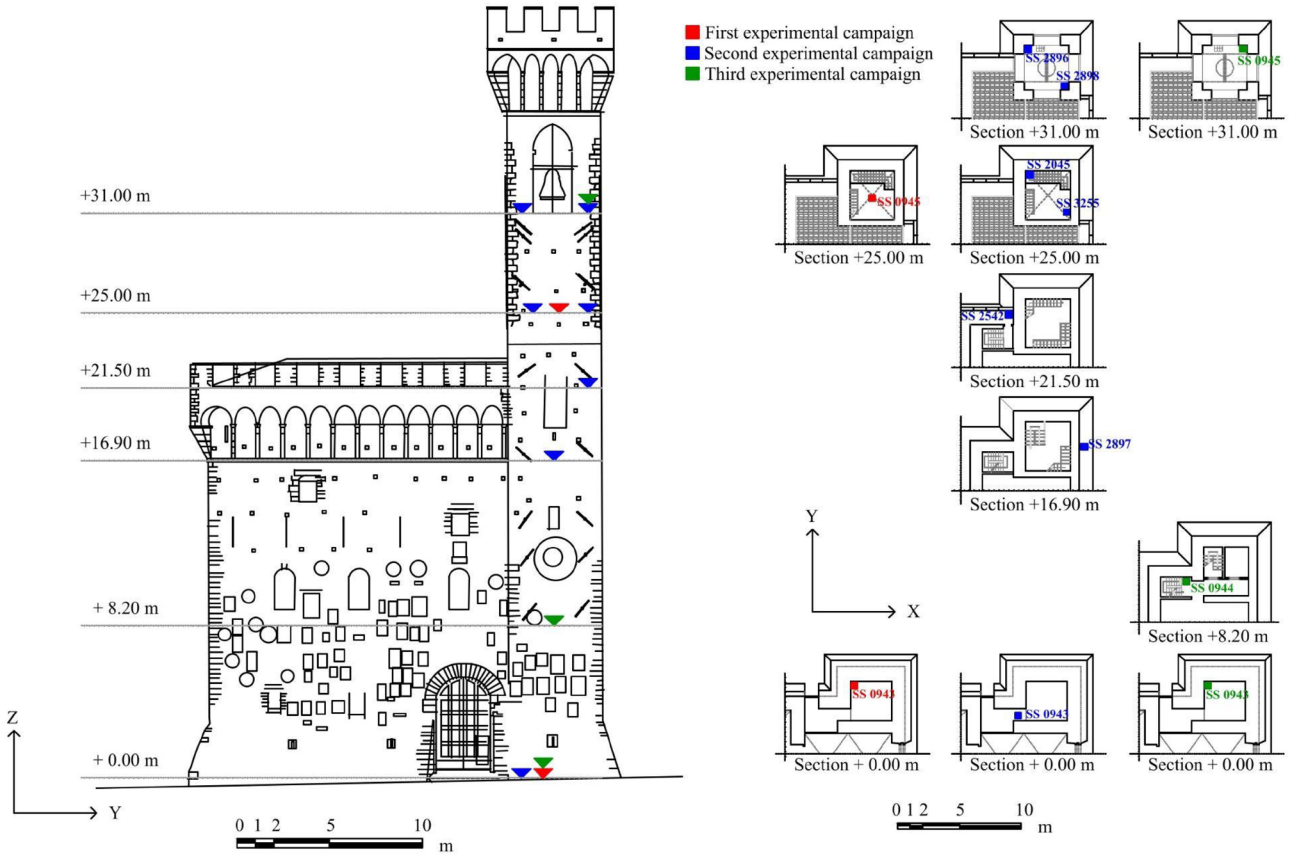

Fig. 6 Geometry of the Tower (length in metres) and experimental setup of the monitoring campaign. Red: position of the seismometers during the first campaign (2019); blue: position during the second campaign (2021); green: position during the third campaign (2023)

event recorded during the monitoring survey was M 3.1, which occurred on 14 December 16:55 UTC.

Figure 7 shows two seismograms recorded on the Tower at level +25 m on 11 December 2019 (M 2.5 earthquake) and on 14 December (M 3.1 earthquake). The peak value of the horizontal velocity recorded during the M 2.5 earthquake is 2.7 mm/s. The M 3.1 earthquake recordings show the saturation of the horizontal components during the most energetic part of the event (yellow box in Fig. 7). Due to technical problems and malfunctioning, the station at the base of the Tower did not record during the seismic events.

The data collected during the first campaign were analysed in the frequency domain to identify the structure's main frequencies. Data analyses were also aimed at describing and comparing the Tower's dynamic behaviour during the most relevant events of the seismic sequence and under ambient vibrations.

2.2.1 Ambient vibrations

Time windows free of seismic events were selected from the data collected by the seismometers. The average hourly spectra (FFT) and average hourly standard spectral ratios (SSR) between the signals recorded at the top and the ground were calculated.

The hourly averages for the spectra and spectral ratios were computed as the average of the quantities calculated on the 30 consecutive 120-s intervals extracted from the hourly recording. The hourly quantities were then averaged to obtain the average FFT and SSR for the monitoring period [4].

Figure 8 shows the average FFTs of the signals recorded by the seismic station at the Tower's top. At low frequencies (< 1 Hz), the spectra are dominated by a broad peak centred at about 0.3 Hz. An additional seismic station installed in the same period on the ground floor of the nearby Scarperia City Hall revealed a similar frequency content; this confirms that the 0.3 Hz peak is not related to structural behaviour but to ambient sources.

Table 1 Earthquakes recorded during the monitoring experiment

Time	Latitude	Longitude	Depth [km]	M	Time	Latitude	Longitude	Depth [km]	*M*
2019-12-09 T15:20:07.80	44.0122	11.2873	9.0	2.5	2019-12-11 T21:19:25.50	44.0035	11.3032	9.4	2.4
2019-12-09 T15:21:35.39	44.0138	11.2900	8.4	2.3	2019-12-12 T17:23:22.44	44.0207	11.3018	8.8	1.8
2019-12-09 T17:09:32.52	44.0083	11.3202	8.0	1.8	2019-12-13 T01:53:55.36	44.0243	11.2818	8.8	2.1
2019-12-09 T17:50:29.84	44.0093	11.3090	8.7	1.8	2019-12-13 T02:58:32.69	44.0208	11.2832	8.7	1.8
2019-12-09 T17:53:52.62	44.0080	11.3143	8.1	2.0	2019-12-13 T03:32:51.00	44.0172	11.2843	8.4	2.1
2019-12-09 T18:09:46.87	44.0080	11.2787	9.0	1.9	2019-12-13 T08:01:18.75	44.0237	11.2843	9.3	1.8
2019-12-10 T02:02:45.63	44.0120	11.3003	9.0	1.8	2019-12-14 T01:39:07.09	44.0158	11.3007	8.7	2.1
2019-12-10 T19:00:53.17	44.0170	11.3067	8.0	2.2	2019-12-14 T03:14:41.45	44.0215	11.2840	9.0	1.8
2019-12-10 T20:47:57.58	44.0123	11.2872	8.9	1.9	2019-12-14 T16:55:53.46	44.0092	11.2973	6.9	3.1
2019-12-11 T04:24:09.10	44.018	11.2987	7.1	2.5	2019-12-14 T21:47:53.31	44.0122	11.3003	8.7	1.8
2019-12-11 T11:47:18.60	44.0072	11.3017	9.9	2.0	2019-12-15 T00:03:52.84	44.0170	11.3077	8.3	2.0

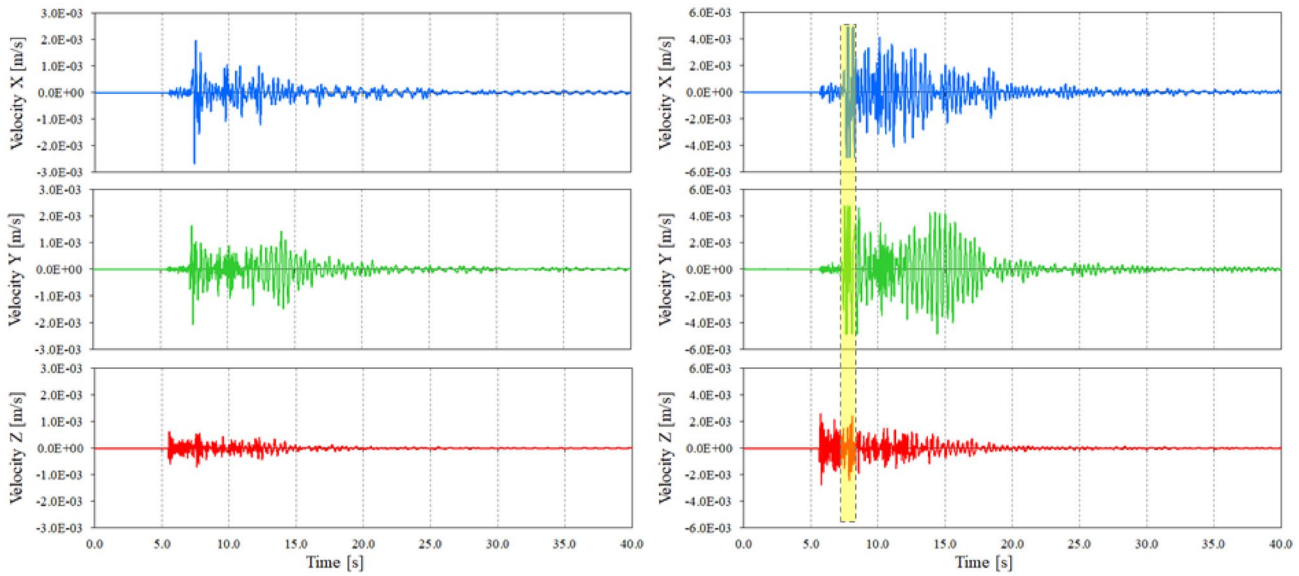

Fig. 7 Velocity waveform of the earthquakes recorded at +25 m on 11 December 2019 04:24 UTC, M 2.5 (left) and on 14 December 2019 16:55 UTC, M 3.1 (right). The region highlighted corresponds to the out-of-scale portion of the signal due to saturation of the sensor

The horizontal spectra at high frequencies (> 1 Hz) show peaks related to the Tower's structural response. To highlight this aspect, the average SSR between the signals recorded on the top and the ground was assessed (Fig. 9). This technique, known as the standard spectral ratio, was first introduced by [26] and is used in seismology to evaluate a relative soil transfer function from the spectral ratio between two nearby stations. Therefore, the spectral ratio between the floor station and the base station (considered as the ground reference station) allows the identification of the main frequencies of the building. As a matter of fact, the SSR technique extracts the frequency content attributable to the ground from the

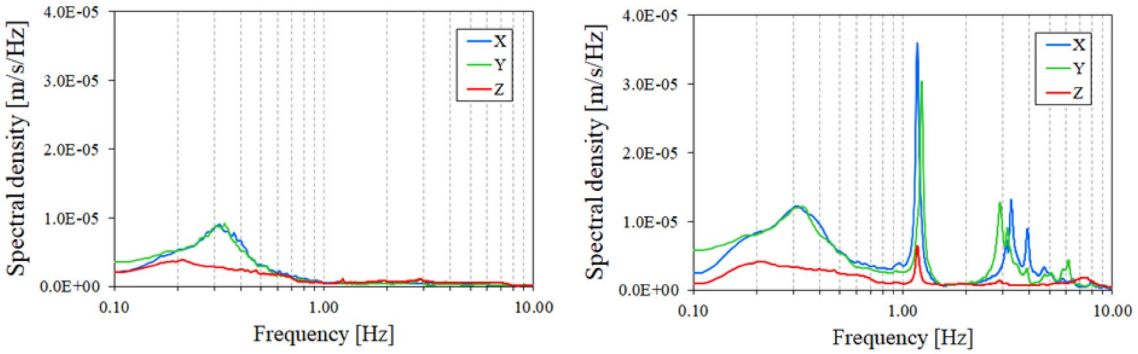

Fig. 8 Average spectra for the Tower of Palazzo dei Vicari. The results are shown for the stations at ground level (left) and top floor (right) for the X, Y and Z components

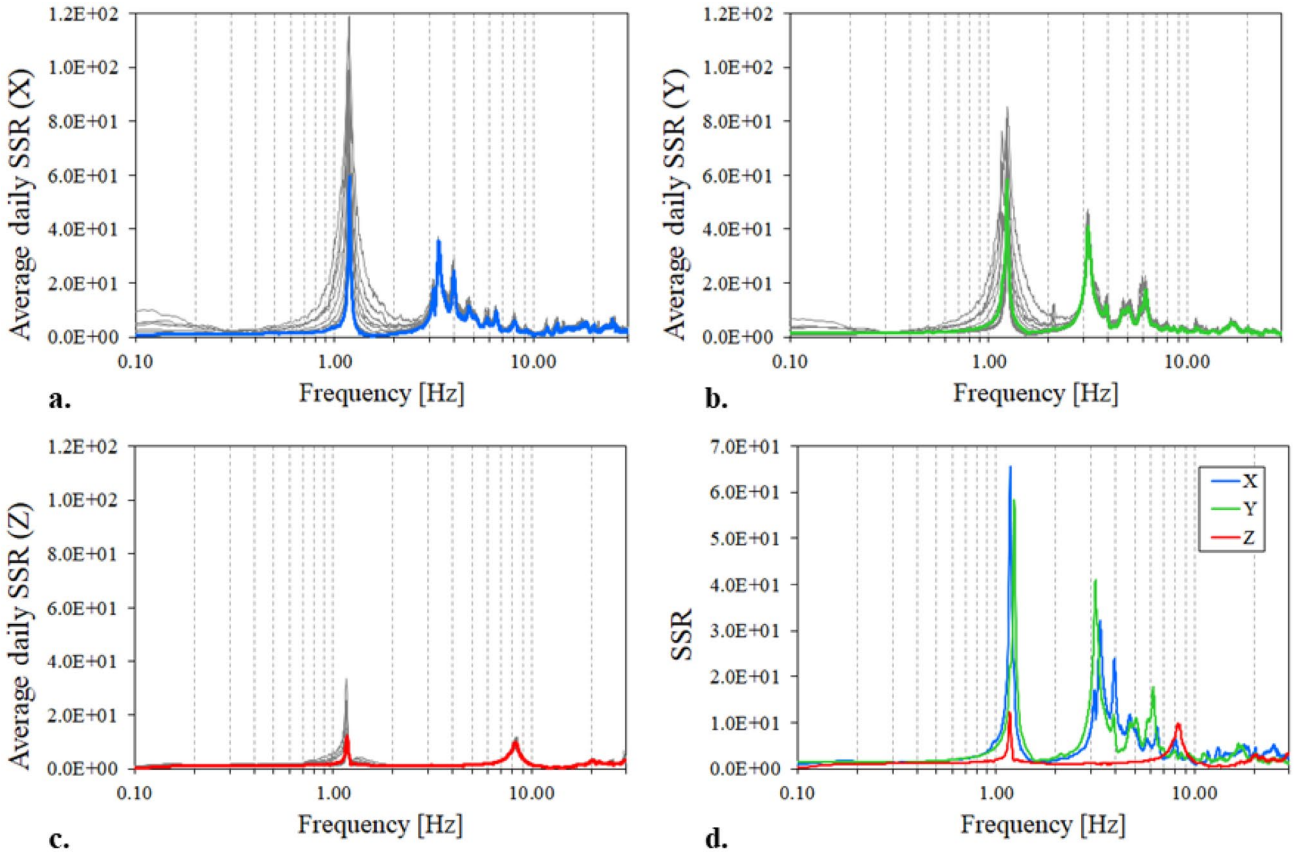

Fig. 9 Average SSR computed on the entire monitoring period between the seismic stations on the top floor and that on the ground for the X (**a**), Y (**b**) and Z (**c**) components (SSR daily average, grey continuous lines; SSR total average, coloured continuous lines). Superposed average total SSR of the X, Y and Z components (**d**)

Table 2 Frequency peaks recognisable in the average SSRs for the Tower of the Palazzo dei Vicari

Component	[Hz]						
X	1.18	3.12	3.34	3.95	4.72	6.5	8.0
Y	1.24	3.16	–	3.91	–	6.2	–
Z	–	–	–	–	–	–	8.2

floor recordings, thus highlighting the frequency content of the structure.

Figure 9a–c shows the daily average (grey lines) and the total average (coloured lines) SSRs computed on the entire monitoring period on the Tower, while in Fig. 9d, the three components are superposed. The peak values of the three average SSRs are listed in Table 2. The first peaks in the X and Y directions (1.18 Hz and 1.24 Hz, respectively) can be easily attributed to the first bending modes of the Tower along the section's principal directions. It is worth noting that they are very close due to the geometry of the Tower's transverse section (Fig. 6). The peak around 3.15 Hz, recognisable in both the X and the Y components, is likely attributable to the first torsional mode. The peak around 0.3 Hz is not visible in Fig. 9; this confirms, being the figure plotted in terms of spectral ratios, that this low-frequency signal is related to ambient sources transmitted to the Tower from the ground.

Figure 9 highlights the remarkable stability of the spectral ratios over the monitoring period, with a small dispersion of the daily curves around the one averaged over the entire monitoring period [19]. This result was expected, as the monitoring period covered about one month, and thus, seasonal temperature variations did not affect the data. Some

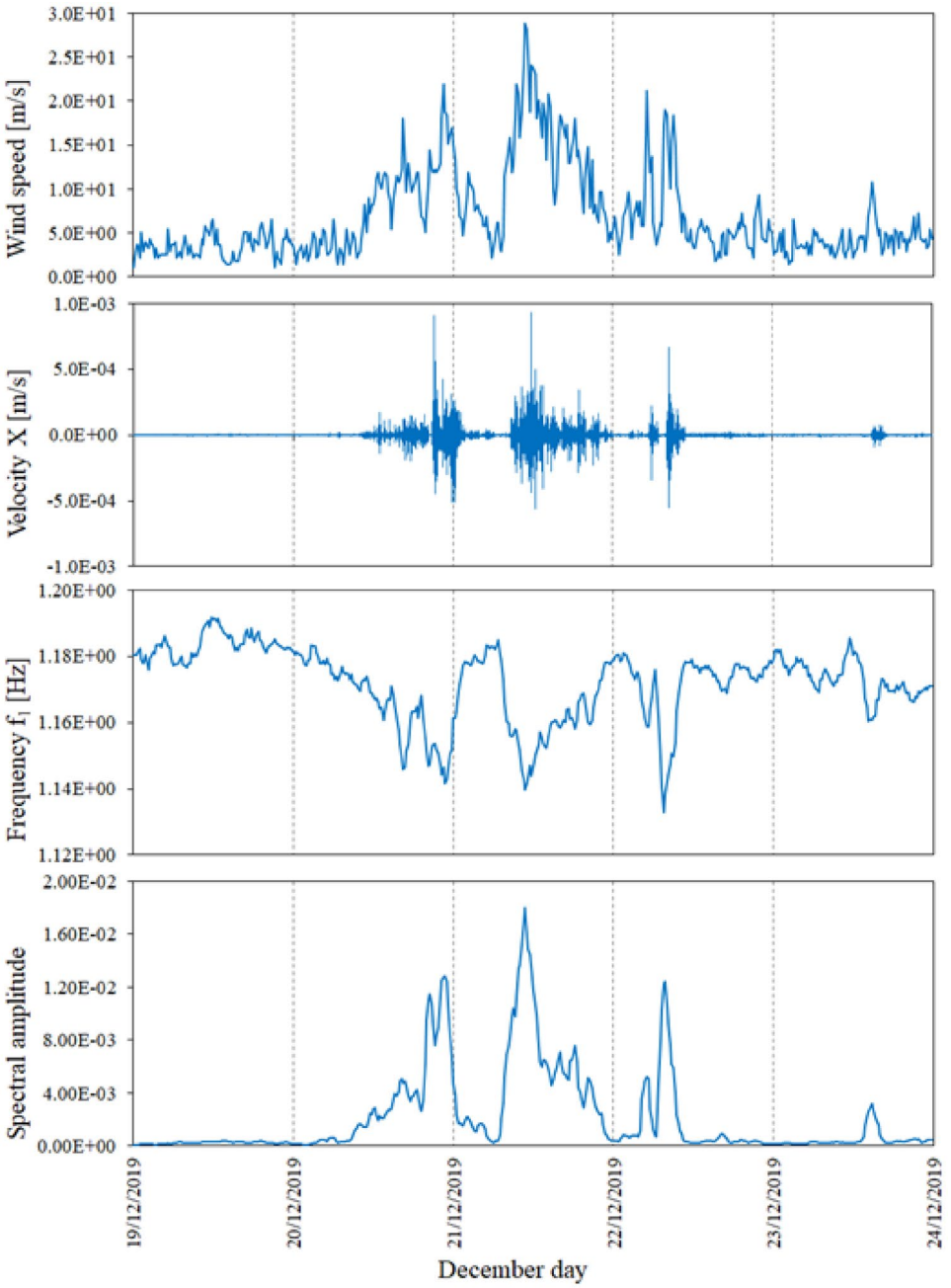

Fig. 10 From the top to the bottom: maximum wind speed (wind gusts) recorded in December 2019 by the Borgo San Lorenzo weather station—http://www.sir.toscana.it/); waveforms recorded on the Tower from 19 to 23 December 2019; the Tower's first frequency trend from 19 to 23 December 2019 and the spectral amplitude of signal recorded inside the Tower

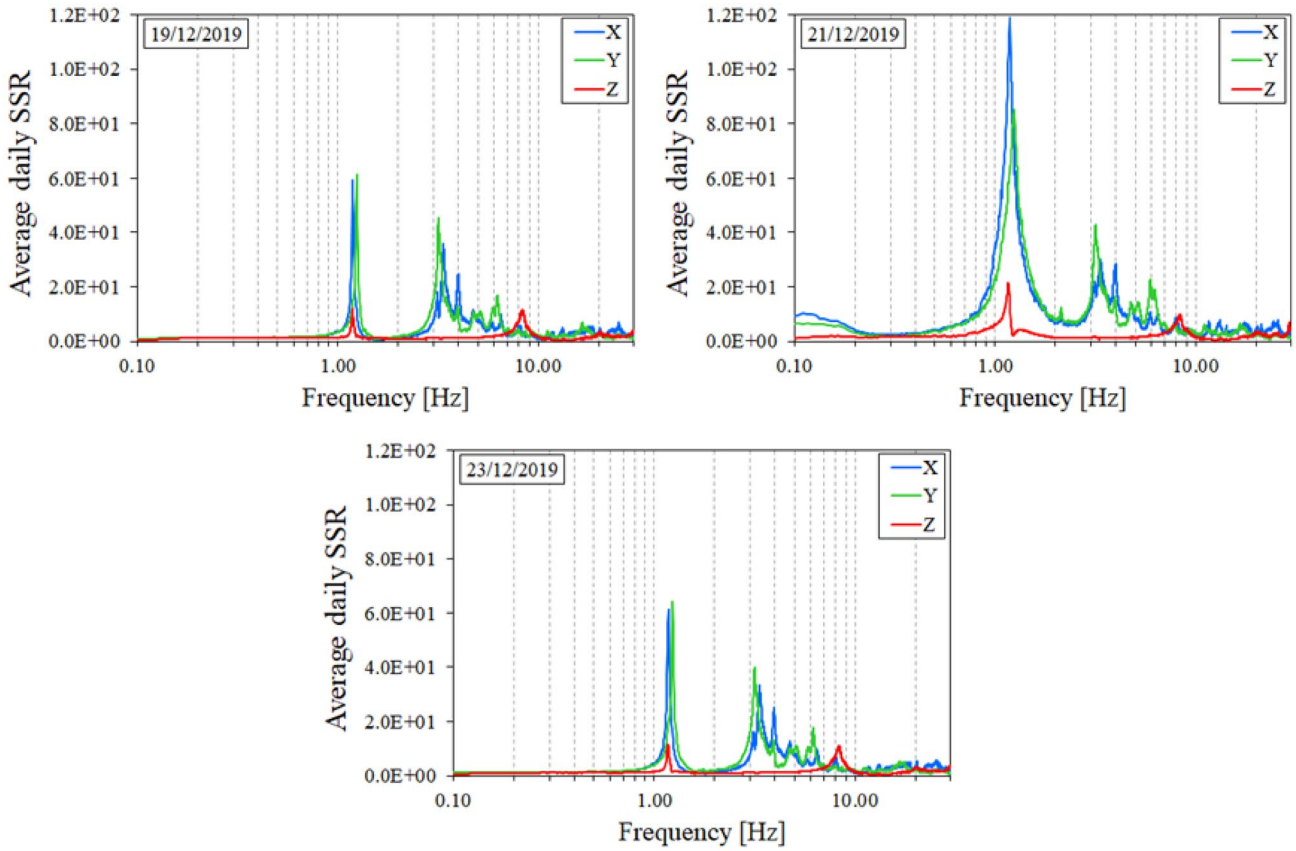

Fig. 11 Daily SSRs computed for 19, 21 and 23 December. The central panel refers to the day (21 December 2019) in which strongest wind gusts occurred

dispersion of the first peak values can be observed during the windiest days (Figs. 10, 11). Figure 10 shows (top) the diagrams of the wind speed (http://www.sir.toscana.it/) recorded by the weather station of Borgo San Lorenzo, a few kilometres away from Scarperia, the seismogram of the X component recorded on the Tower from 19 to 23 December 2019, the trend of the Tower's fundamental frequency over the same days and, finally, the spectral amplitude of the signal in the X direction. One-minute signals have been stacked from the recordings and processed to follow the fundamental frequency over time. Figure 10 shows a clear correlation between the energy content of the signal and the frequency values; in particular, the frequency decreases when the spectral amplitude increases [35].

Figure 11 shows the SSRs for 19, 21 and 23 December. The major energy content of the signal during the windiest day is evident in the figure.

It is worth noting the strong amplification along the height of the transverse oscillations of the Tower. The amplitude of the spectral ratio is on the order of 70 on the occasion of the strongest gusts (21 December) (Fig. 11).

An estimation of the damping ratio from the analysis of the Tower's free vibrations has been performed. The *geopsy tools* (www.geopsy.org) [64] have been used here for damping calculation. The software applies the Random Decrement Technique (RDT) [21, 54] to the vibration recordings. Considering the suggestions in the literature (see, for example, [24, 26, 45]), the calculations have been performed over an entire daily recording, free as much as possible from relevant transients. The daily signal recorded by the top station has been divided into 30 seconds shorter signals that were then band-pass filtered in the range of 0.5–1.5 Hz. The damping values obtained for the Tower are very low, on the order of 0.6%.

2.2.2 Earthquake data

Twenty-two seismic events with a magnitude greater than 1.8 (Table 1) were selected from the seismic sequence that struck the Mugello area during the monitoring period to compare the dynamic behaviour of the Tower under earthquake and ambient vibrations. The earthquakes in Table 1 were divided into two groups according to the magnitude supplied by the INGV database: $M \leq 2.5$ and $M > 2.5$. The second class consists of the strongest event recorded

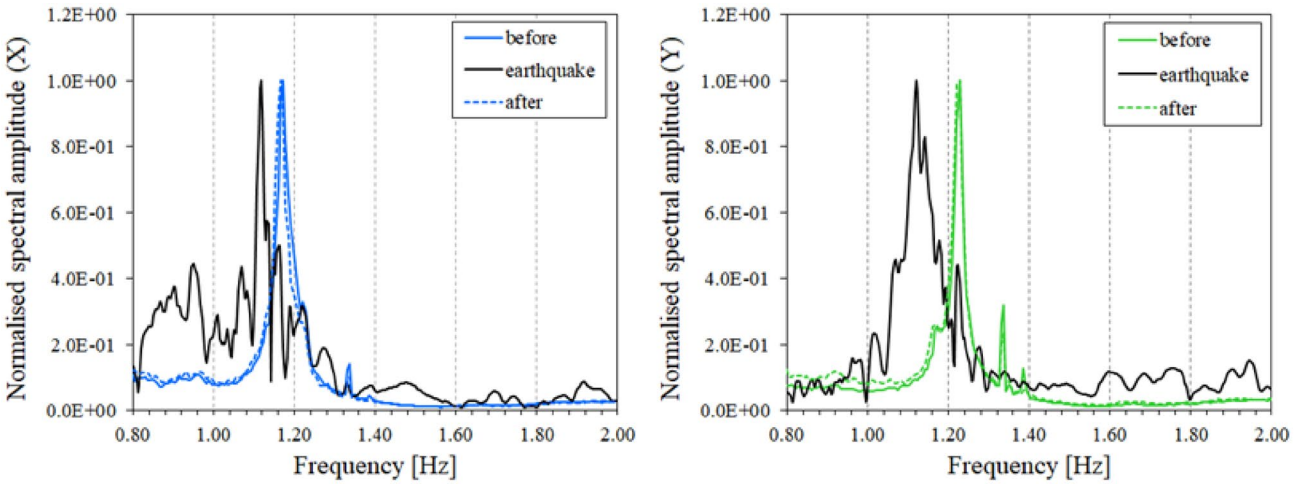

Fig. 12 Comparison between the average FFTs computed before (continuous line), during (continuous black) and after (dashed line) the earthquake of 14 December, M 3.1, for the station at the top of the Tower. From left to right: X and Y directions

during the monitoring period, M 3.1, which occurred on 14 December.

Unfortunately, a technical failure at the Tower's ground-level station resulted in a data loss from 9 to 16 December; no earthquakes larger than M 1.8 occurred after that date. This failure made using the SSR technique impossible; the FFTs of the signal recorded by the upper floor's station before, during, and after the M 3.1 earthquake were then computed (Fig. 12).

More precisely, two signals have been extracted before and after the earthquake. The average FFT over 120 consecutive signal intervals was computed and compared to that obtained by processing the signal recorded during the seismic event. The figure shows a shift of the peaks related to the first bending frequency during the earthquake. The Tower's dynamic behaviour before and after the earthquake remains substantially unchanged regarding frequencies. The authors have observed this phenomenon on similar monuments [9] during low-to-moderate events.

Figure 13 shows, for the M 3.1 event, the trend versus time of the Tower's first and second frequencies (top), the corresponding spectral amplitudes along the X and Y direction (middle), and the time-history of the event in terms of velocities (bottom). As for Fig. 10, one minute signals have been stacked from the recordings and processed via FFT to follow the frequencies over time. The frequency decay during the earthquake [36] is evident in the figures (yellow region).

2.3 Second experimental campaign (June 2021)

A second experimental campaign was conducted on 15 June 2021 to improve the dynamic identification of the Tower, under ambient vibrations. Seven three-axial velocity transducers, recording with a sampling frequency of 100 Hz, were installed at different heights, from the base to the bell chamber (see Fig. 6). The signals were processed through the stochastic subspace identification covariance driven (SSI-cov) method [15], implemented in the MACEC code [53]. The algorithm relies on the hypotheses of the OMA, which models the input as an unknown white noise signal and processes the output-only response of the system. Table 3 shows the results obtained in terms of natural frequencies, standard deviation and Modal Phase Collinearity (MPC). These frequencies have been confirmed by FE calibration and are also recognisable in the signals recorded in the first experimental campaign. A good agreement is found between the results shown in Table 2 (first experimental campaign) and Table 3. Figure 14 shows the first four mode shapes of the Tower calculated by the MACEC code. The damping values computed confirm the low values reported in Sect. 2.2.1.

2.4 Third experimental campaign (September 2023)

An M 4.9 earthquake was recorded in the Mugello area on 18 September 2023. The earthquake was located at about 20 km NW from Scarperia, near the city of Marradi. The seismic sequence triggered by the event lasted more than one month producing about 700 events with magnitude from 0.5 to 4.9. The most energetic part of the sequence occurred in the first days of its evolution. All the events with magnitude greater than 3.0 occurred within two days of the mainshock. The event with the highest magnitude (M 2.6) recorded by the seismic stations occurred on 21 September 08:35 UTC.

Three seismic stations were installed inside the Palazzo and Tower from 20 September to 4 October 2023 (Fig. 6). One station was installed at the base, a second station at the first floor, the third one at the top terrace of the Tower.

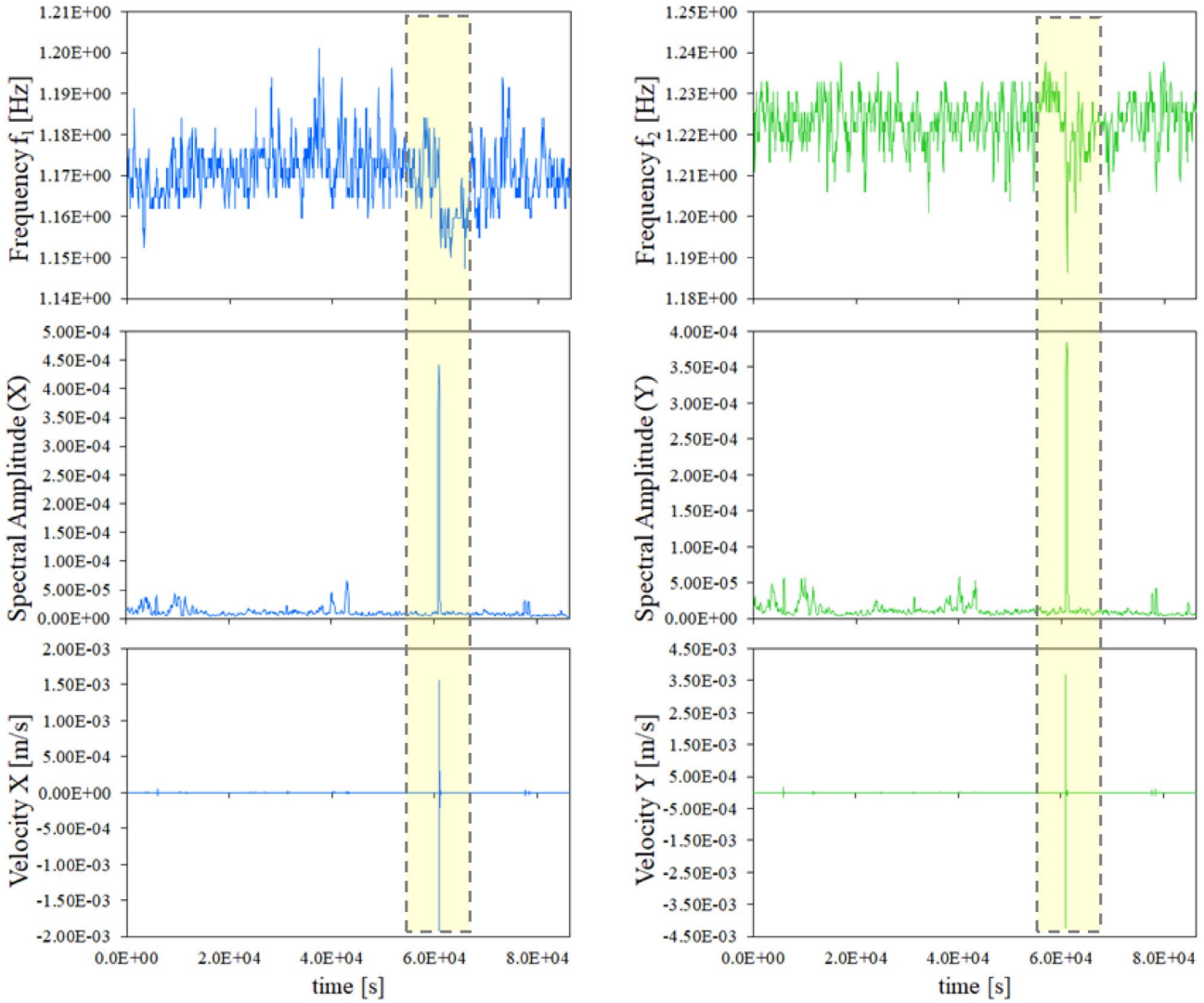

Fig. 13 From the bottom to the top: time-histories of the velocities recorded in X and Y direction during the earthquake of 14 December, M 3.1; spectral amplitude of the signals; trend of the first (X) and second (Y) Tower's frequencies vs. time. The yellow region highlights the earthquake's effects

Table 3 Natural frequencies and mode shapes of the Tower of the Palazzo dei Vicari

Mode shape	SSI-cov	
	f [Hz]	MPC
1 (Bending X)	1.22 ± 0.002	0.95
2 (Bending Y)	1.25 ± 0.002	0.91
3 (Torsional)	3.01 ± 0.011	0.90
4 (Bending X)	3.42 ± 0.121	0.97

Figure 15 reports the X, Y and Z velocities recorded at the base (black) and at the top (blue, green and red) of the Tower on 21 September at 08:35. Strong amplification of the signal along the Tower's height can be observed, particularly in the X and Y directions, along which the signal at the top of the Tower is more than four times that recorded at the base. The maximum ground velocity recorded at the base is on the order of 0.1 mm/s, while the maximum value recorded at the top is 0.23 mm/s.

In Sect. 3.3, the signal recorded at the base has been assigned to a FE model of the Tower to investigate its dynamic behaviour and compare experimental and numerical results.

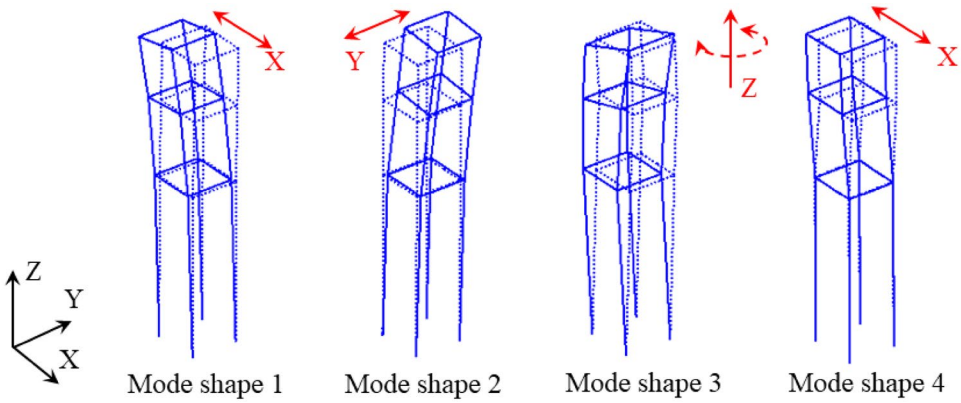

Fig. 14 Mode shapes of the Tower resulting from the dynamic identification

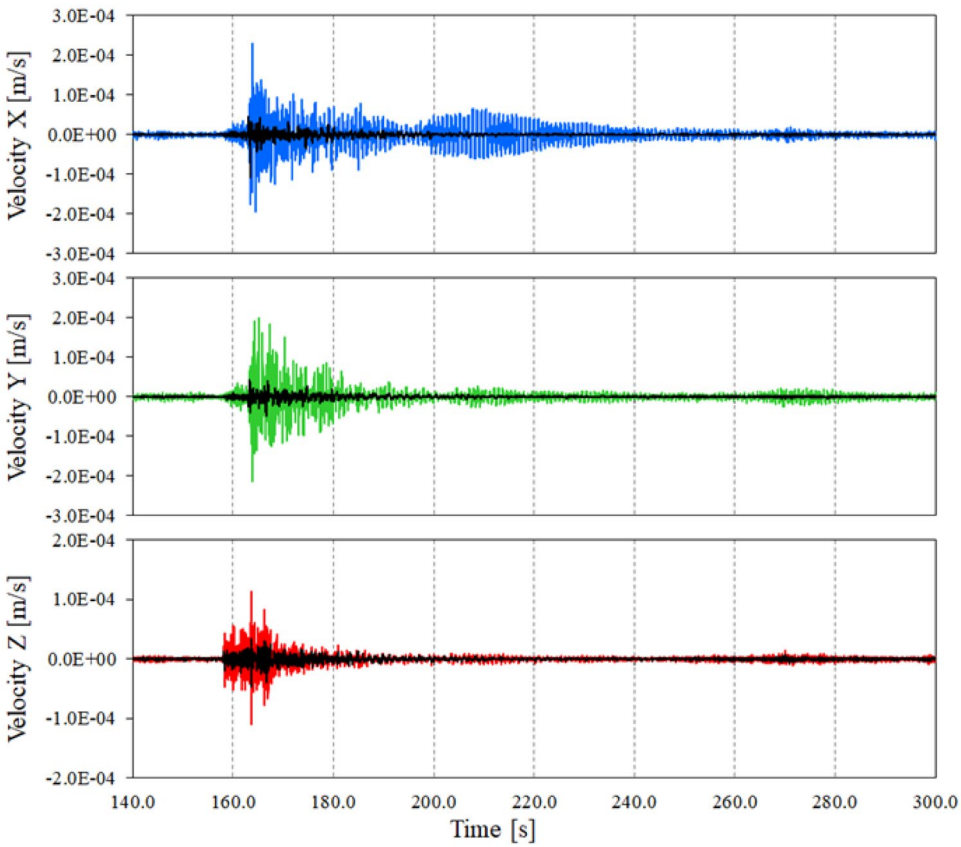

Fig. 15 Velocity waveform of the earthquake recorded inside the Tower on 21 September 2023 08:35 UTC, M 2.6 (continuous black line, signals recorded at the Tower's base; continuous coloured line, signals recorded at the top)

3 Numerical modelling

This section describes the numerical simulations conducted on the Tower via the NOSA-ITACA code. Section 3.1 is devoted to a brief description of the code and its main features. Section 3.2 describes the FE model of the Tower calibrated using the experimental frequencies calculated in Sect. 2. In Sects. 3.2 and 3.3, the results of dynamic and pushover analyses conducted on the Tower's model are presented and discussed.

3.1 The NOSA-ITACA code

The NOSA-ITACA program [34], developed by ISTI-CNR for the nonlinear analysis and calibration of masonry structures (www.nosaitaca.it/software), combines the finite element (FE) solver NOSA and SALOME, an open-source interactive graphic platform for pre- and post-processing operations. The software can be used for FE model updating, static and dynamic analysis of structures made of linear elastic and masonry materials and thermomechanical analysis in the presence of thermal loads. Moreover, it allows modelling

restoration and reinforcement operations on constructions of architectural interest.

The code adopts the constitutive equation of masonry-like materials [39] and models masonry as a homogeneous isotropic nonlinear elastic material with zero or weak tensile strength ($\sigma^t \geq 0$) and infinite or bounded compressive strength ($\sigma^c > 0$).

Assumptions underlying the model are that the infinitesimal strain tensor $\mathbf{E}$ is the sum of an elastic part $\mathbf{E}^e$, a fracture part $\mathbf{E}^f$ and a crushing part $\mathbf{E}^c$ and that the stress tensor $\mathbf{T}$ depends linearly on the elastic part, $\mathbf{T} = \mathbb{C}[\mathbf{E}^e]$, with $\mathbb{C}$ the isotropic fourth-order elasticity tensor containing the mechanical properties of the material (the Young's modulus and the Poisson' ratio). The symmetric tensors $\mathbf{T}$, $\mathbf{E}^f$ and $\mathbf{E}^c$ satisfy suitable orthogonality conditions; moreover, $\mathbf{T} - \sigma^t\mathbf{I}$ (with $\mathbf{I}$ the identity tensor) and $\mathbf{E}^c$ are negative semidefinite and $\mathbf{T} + \sigma^c\mathbf{I}$ and $\mathbf{E}^f$ are positive semidefinite.

NOSA-ITACA relies on a finite-element formulation of the differential equations governing the statics and dynamics of masonry structures. The nonlinear system obtained by discretizing the structure into finite elements is solved via the Newton–Raphson method, which involves the tangent stiffness matrix $\mathbf{K}_T$. The numerical solution to the dynamic problem is based on the Newmark method.

Experimental dynamic monitoring campaigns revealed the dependence of natural frequencies on structural changes and damages [32, 52], as well as on environmental factors, such as temperature and humidity [6, 32].

NOSA-ITACA has been thus enhanced to use experimental data such as frequencies and mode shapes to calibrate the FE counterpart of masonry buildings and model the influence that both the nonlinear behaviour of the masonry material and the presence of cracked regions can have on the dynamic properties of masonry structures.

Given the structure under examination, discretised into finite elements, and given the mechanical properties of the constituent materials together with the kinematic constraints and loads acting on the structure, the procedure implemented in NOSA-ITACA encompasses the following two stages:

1. The solution to the nonlinear equilibrium problem of the structure is calculated and the tangent stiffness matrix $\mathbf{K}_T$ to be used in the next step is evaluated.
2. A modal analysis about the equilibrium solution is performed employing the tangent stiffness matrix $\mathbf{K}_T$ calculated in the last iteration of stage 1 before the convergence is reached. The generalised eigenvalue problem

$$\mathbf{K}_T\mathbf{v} = \omega^2\mathbf{M}\mathbf{v} \tag{1}$$

is then solved. In (1), $\mathbf{K}_T$ and $\mathbf{M} \in \mathbb{R}^{n\times n}$ are the symmetric and positive definite tangent stiffness and mass matrices of the finite-element assemblage. The integer n is the total number of degrees of freedom of the system and is generally very large since it depends on the discretisation of the problem. Solving (1) provides the first q smallest natural frequencies $f_i = \omega_i/(2\pi)$ and mode shapes $\mathbf{v}^{(i)}$ of the cracked structure, with $i = 1, \ldots, q$, $q << n$. In the linear perturbation approach, the tangent stiffness matrix $\mathbf{K}_T$ replaces the elastic stiffness matrix $\mathbf{K}$ used in the standard modal analysis, in which the materials constituting the structure are linear elastic.

The nonlinear model updating implemented in NOSA-ITACA can be formulated as an optimisation problem by assuming that the tangent stiffness and mass matrices are functions of the parameter vector $\mathbf{x}$, containing the Young's moduli, tensile strength and density masses of the constituent materials. The goal is to determine the optimal value of $\mathbf{x} \in \mathbb{R}^p$ that minimises the objective function $\phi(\mathbf{x})$ involving q experimental frequencies to match, within a p-dimensional box $\Omega = [a_1, b_1] \times \ldots \times [a_p, b_p]$

$$\phi(\mathbf{x}) = \sum_{i=1}^{q} w_i^2 \left(f_i^{exp} - f_i(\mathbf{x})\right)^2 + w_{q+i}^2 \left(1 - \gamma_i(\mathbf{x})\right)^2 \tag{2}$$

with f_i^{exp} the experimental frequencies, $f_i(\mathbf{x})$ the numerical frequencies obtained from (1), $\gamma_i(\mathbf{x})$ the modal assurance criterion (MAC) indicators and $w_i \in \mathbb{R}$ suitable weights, $i = 1, \ldots, q$. The minimum problem that must be solved to calibrate the FE model is a nonlinear least squares problem: the objective function, having form (2), is nonlinear as the frequencies $f_i(\mathbf{x})$ depend nonlinearly on the vector $\mathbf{x}$ of material properties. In addition, another source of nonlinearity of $\phi(\mathbf{x})$ is the dependence of $\mathbf{K}_T(\mathbf{x})$ (and then of $f_i(\mathbf{x})$) on the solution of the nonlinear equilibrium problem in stage 1 [33].

3.2 Finite-element model calibration

An FE model of the Tower was created with NOSA-ITACA. The mesh of the structure, assumed to be perfectly clamped at the base (no information related to the foundations and the soil is available, so the soil–structure interaction is neglected), is shown in Fig. 16 and consists of 16,002 isoparametric brick and truss elements (element no. 1 and no. 35 of the software library) with 20,867 nodes, for a total of 62,601 degrees of freedom. In a first approximation, the presence of the adjacent palace is modelled via elastic springs with stiffness k_x and k_y as a detailed survey of the building and information regarding the connection to the surrounding tower-palace complex are not available. We assume that the Tower is subjected to the self-weight and divided into five portions constituted by different masonry materials with Young's modulus E_i ($i = 1, \ldots, 5$), $\nu = 0.2$, uniform mass density 2000 kg/m^3, tensile strength $\sigma^t = 0$

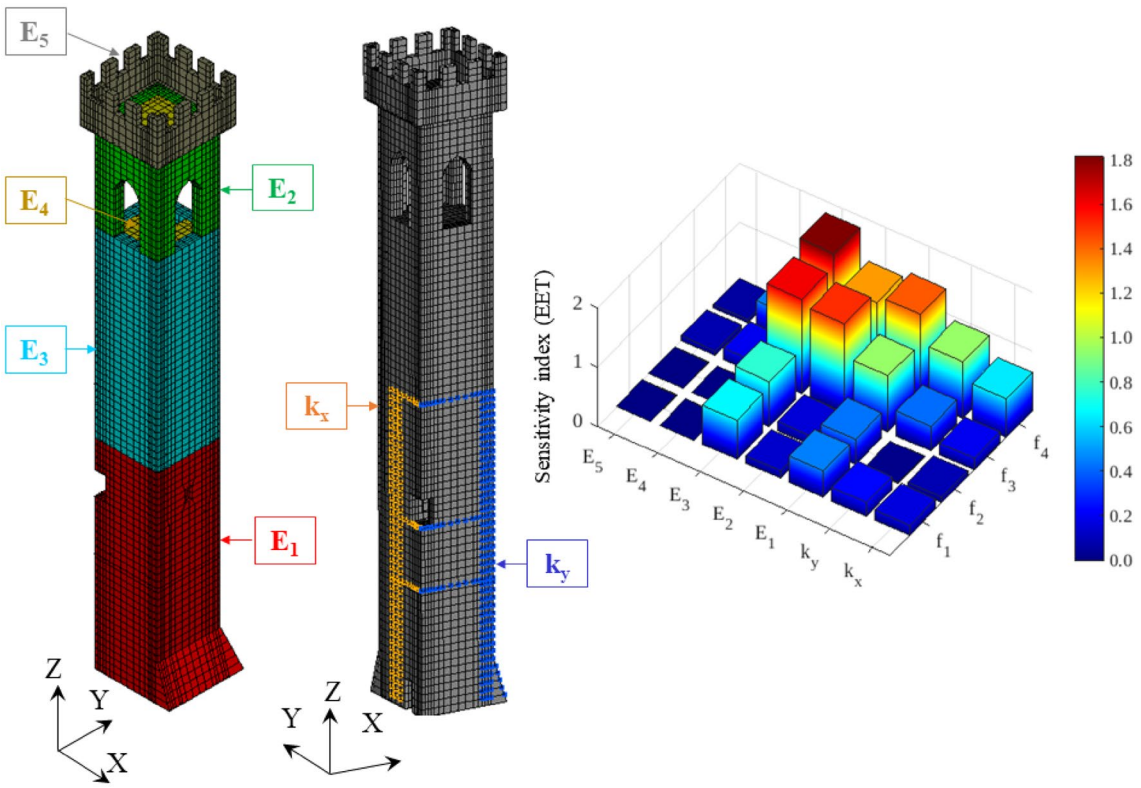

Fig. 16 FE model of the Tower (left) and sensitivity indexes calculated via GSA (right)

Table 4 Optimal parameter values and numerical frequencies calculated by NOSA-ITACA, experimental frequencies, relative errors and MAC values

	f_i^{exp}[Hz]	f_i[Hz]	$\lvert\Delta f_i\rvert$ [%]	MAC
Mode 1	1.22	1.22	0.00	0.99
Mode 2	1.25	1.25	0.00	0.99
Mode 3	3.01	3.02	0.33	0.73
Mode 4	3.42	3.91	14.32	0.93
k_x [N/m]	k_y [N/m]	E_1 [MPa]	E_2 [MPa]	
905,305	621,992	4020	700	

MPa and compressive strength $\sigma^c = 1$ MPa [48]. In particular, the portions are the lower part contained in the palace (E_1), the bell chamber (E_2), the part between the palace and the bell chamber (E_3), the vaults (E_4) and the roof (E_5).

A Global Sensitivity Analysis (GSA) has been performed through the SAFE Toolbox [49] coupled with NOSA-ITACA to investigate how variations in the input (Young's moduli of the constituent materials and springs' stiffness) influence the output of the numerical model (the natural frequencies). The sensitivity indexes, evaluated by SAFE and adopting the Elementary Effects Test method, are shown in Fig. 16 for the first four frequencies and the parameters vector (k_x, k_y, E_1, E_2, E_3, E_4, E_5). As it is possible to note, the first two frequencies are slightly dependent on E_1 and E_3, the third frequency is influenced mainly by E_2 and E_3, and by E_1 and k_y to a minor extent. Finally, the fourth frequency mostly depends on E_1 and E_3, with a lower influence of k_x, k_y and E_2. Young's moduli E_4 and E_5 characterising the vaults and the roof seem irrelevant from a dynamic point of view.

Given the results of GSA, the nonlinear model updating sketched in Sect. 3.1 has been conducted by minimising the objective function in (2) with $q=4$, $p=4$, $\mathbf{x}=(k_x, k_y, E_1, E_2)$, f_i^{exp} reported in Table 3, $w_i = 1/f_i^{\text{exp}}$, $i=1, 2, 3, 4$, $w_i = 0.1$, $i=5, 6, 7, 8$ and assuming that $E_5=E_4=E_3=E_1$.

The optimal values of $\mathbf{x}$ and the numerical frequencies are reported in Table 4, along with the experimental ones, the corresponding relative error and MAC (Modal Assurance Criterion) values. Table 4 highlights a strong agreement between the numerical and experimental frequencies, with a maximum relative error of 0.33%, except for the fourth frequency. In terms of MAC values, however, the correlation between the third numerical and experimental mode shapes is low, although still acceptable, especially considering the limited number of sensors used for the dynamic identification.

In the light of previous considerations, the calibrated model of the Tower has been adopted to conduct the nonlinear dynamic analysis described in Sect. 3.3 and the pushover analyses reported in Sect. 3.4.

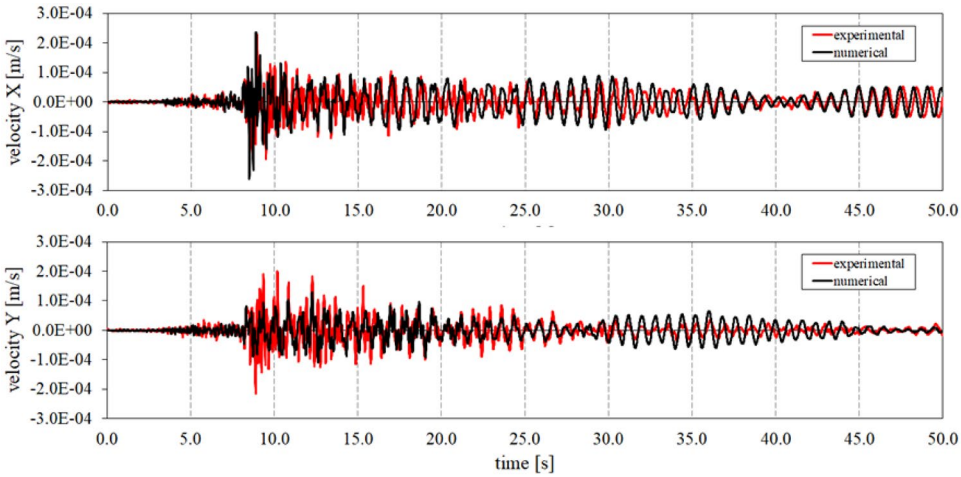

Fig. 17 Earthquake of 21 September 2023 08:35 UTC: velocities (m/s) in the X (top) and Y (bottom) directions versus time (s) recorded by the seismic station SS0945 (red) and calculated by NOSA-ITACA (black)

Table 5 Comparison between experimental and numerical PCPV

Station	PCPV direction	Experimental PCPV [mm/s]	Numerical PCPV [mm/s]	Relative error [%]
SS0945	X	0.229	0.236	−3.06
SS0945	Y	0.199	0.129	35.18

3.3 Nonlinear dynamic analysis

The calibrated model of the Tower is used to conduct a nonlinear dynamic analysis by assigning the signals of the M 2.6 seismic event recorded by the station at the Tower's base on 21 September 2023 08:35 (Fig. 15), to the model and comparing experimental and numerical velocities.

After the dead loads were assigned, the seismic signal recorded was applied to the model, whose numerical response to the dynamic excitation was compared to that recorded on the Tower by the station SS0945. The duration of the quaking was 50 s, and the time step for numerical integration was set at 0.01 s.

The presence of damping in the equations of motion is modelled by the damping matrix, which depends on the elastic stiffness and mass matrices according to the Rayleigh assumption [20]. A damping ratio of 0.4% has been used for the first two mode shapes. This value results from a numerical calibration aimed at fitting the experimental velocities and substantially agrees with the damping values estimated in the experimental campaigns.

Figure 17 shows the velocity in the X and Y directions vs time recorded by the instrument SS0945 placed at + 31.00 m (red line), together with that calculated by NOSA-ITACA (black line).

For comparison, Table 5 reports the peak component particle velocities (PCPV) (PCPV denotes the maximum absolute value of the experimental or numerical velocities

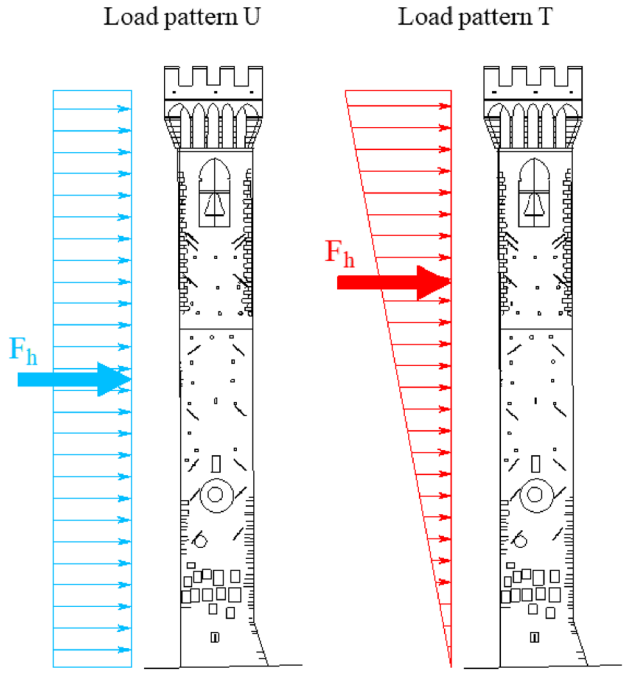

Fig. 18 Load patterns used in the pushover analyses

components) calculated by NOSA-ITACA and their experimental counterparts. As shown in Fig. 17 and highlighted by Table 5, the numerical analysis can fit the recorded experimental time-histories and estimate the peak velocity values reached along the X direction by the structure at the monitored point with an excellent approximation. On the contrary, the numerical analysis underestimates the velocity value in the Y direction, probably due to the choice adopted for modelling the boundary conditions.

The low value of the modal damping is highlighted by the long Tower's response after the transient induced by the earthquake (see Fig. 17). A beating effect is also visible in the data (both in the experimental and numerical results),

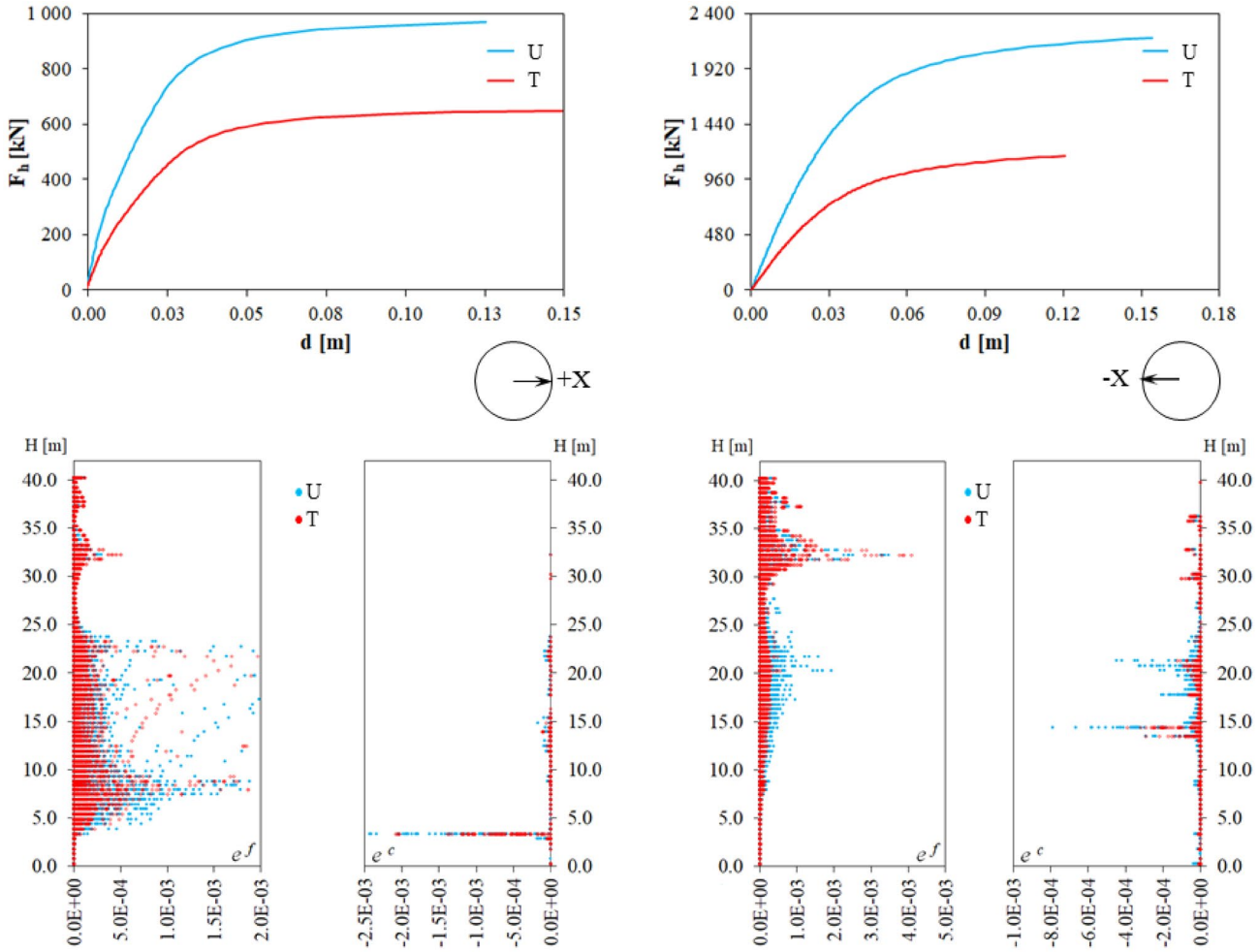

Fig. 19 Pushover analysis. Results for load patterns U and T applied in the + X and − X directions: capacity curves (up); cracking and crushing distributions (bottom)

with an energy exchange between the modes in the X and Y directions. It is worth noting that the first two Tower's frequencies (corresponding to bending in the X and Y directions) are very close, and the oscillations in the two directions could be coupled via the third torsion mode. A similar phenomenon has also been observed for the Asinelli Tower in Bologna [11].

3.4 Pushover analysis

Pushover analyses have been conducted to determine the Tower's performance under seismic actions, as reported in many applications to masonry towers [44, 55].

The horizontal loads (see Figs. 18, 19, 20, 21, 22, 23) were applied in the X and Y directions and along the two bisectors of the (X, Y) plane. For each direction, two different horizontal loading patterns were chosen, as recommended by the Italian Code [47]: a uniform distribution (U) and an inverted triangle distribution (T). Thus, 16 load conditions were considered by applying each load distribution along the following directions: + X, − X, + Y, − Y, + X + Y, − X − Y, − X + Y, + X − Y. In order to visualise the cracked and crushed portions of the Tower effectively, the following elemental ratios:

$$e^f = \frac{1}{V}\int tr\left(\mathbf{E}^f\right)dv, e^c = \frac{1}{V}\int tr(\mathbf{E}^c)dv \tag{3}$$

between the integral of the trace of the fracture and crushing strain on the element and the element's volume V were considered.

Figures 19, 20, 21, and 22 show the results in terms of capacity curves and cracking and crushing distributions. In the figures, d is the displacement of the control node (coinciding with the centre of mass of the roof floor), and the ratios e^f and e^c are plotted against the distance H from the Tower's base ($H \in [0, H_T]$, with $H_T = 40$ m the height of the Tower), for the different load conditions.

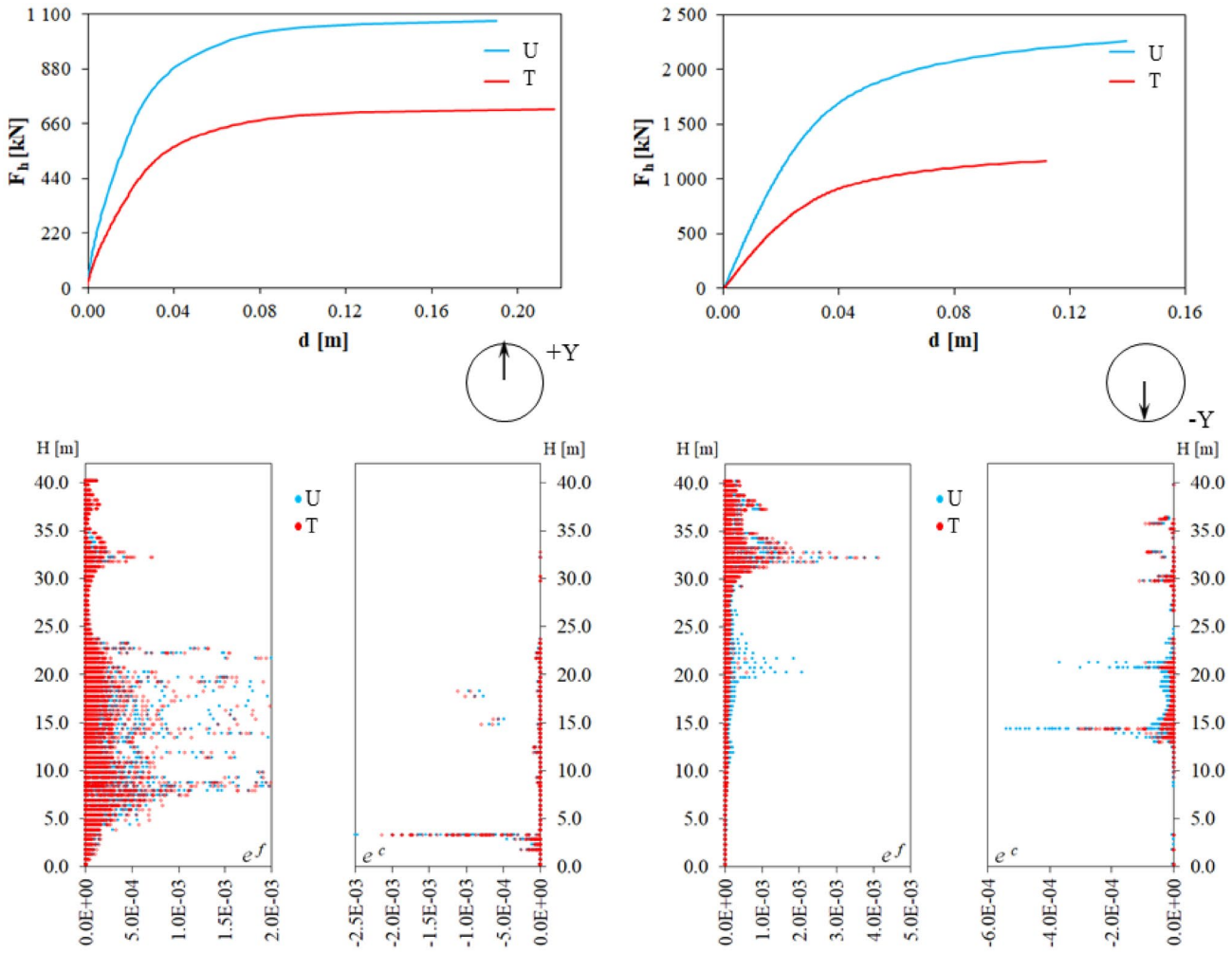

Fig. 20 Pushover analysis. Results for load patterns U and T applied in the + Y and − Y directions: capacity curves (up); cracking and crushing distributions (bottom)

Figure 23 summarises the results of the analyses in terms of: collapse load F_h normalised to the Tower's self-weight W (a.); ratio (percentage) between the displacement d of the control node and the total height H_T of the Tower (b.); bell chamber's interstory drift (percentage) (Δ_c is the displacement of the top with respect to the base of the bell chamber, $h_c = 9$ m is the bell chamber's height) (c.).

The analysis of the previous figures allows us to make the following remarks:

- The load patterns affect the capacity curve in terms of collapse load, and the inverted triangle load pattern is the most unfavourable.
- The asymmetry of the boundary conditions and the cross-section affects the response of the Tower.
- In terms of collapse load, the most critical direction is + X, with F_h in the order of 0.05% of the Tower's weight.
- The worst condition in terms of displacements occurs along the + X + Y direction, adopting the T load pattern.
- The most significant differences between the results of the U and T load distribution occur along the bisector of the first and third quadrants.
- The maximum displacement of the control node is in the order of 0.6% of the total Tower's height, the interstory drift of the bell chamber is in the order of 0.9%.

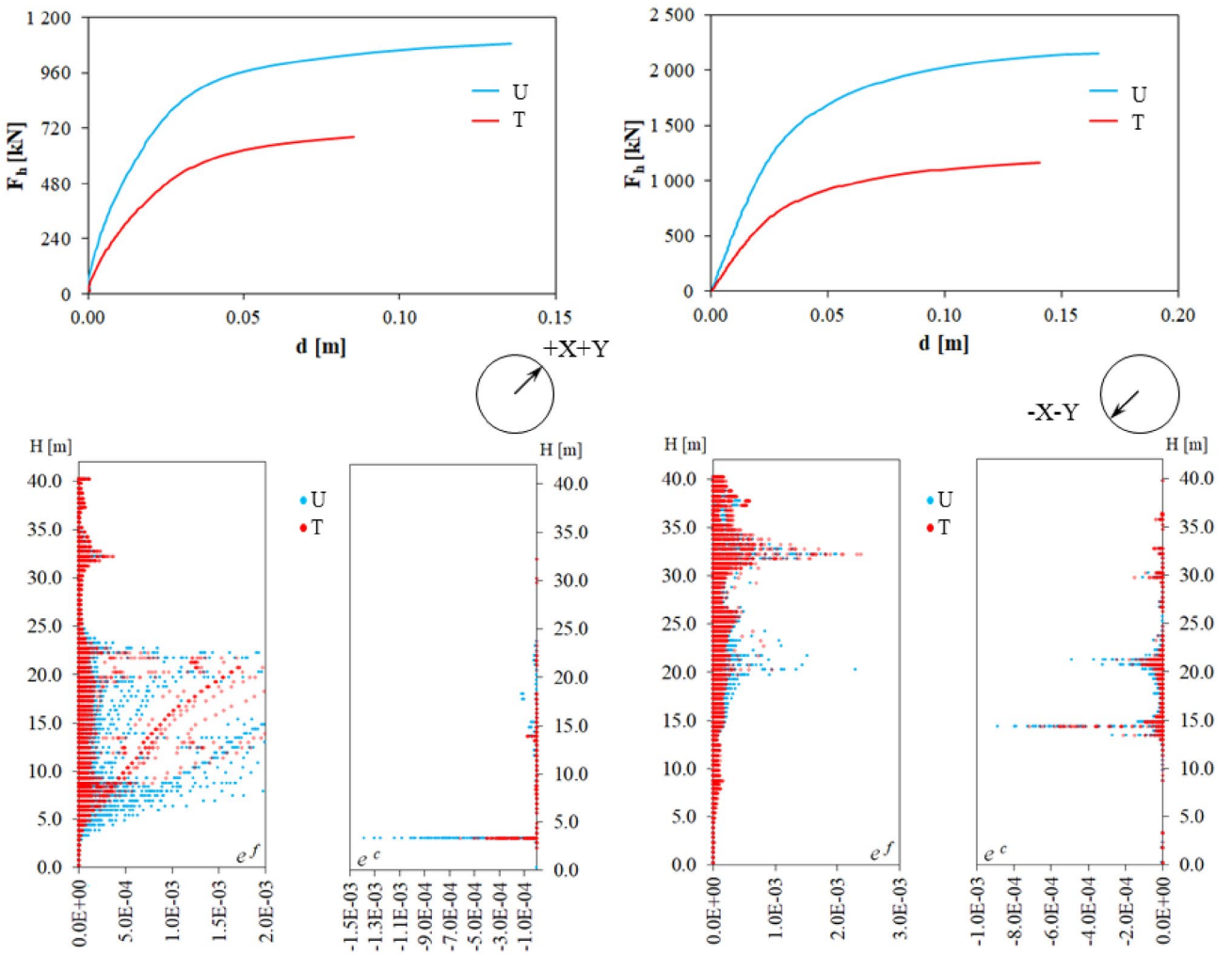

Fig. 21 Pushover analysis. Results for load patterns U and T applied in the + X + Y and − X − Y directions: capacity curves (up); cracking and crushing distributions (bottom)

– The cracking and crushing pattern of the bell chamber is the same for the U and T distribution.

Figure 24a and b shows the crack and crushing patterns of the Tower when subjected to load pattern T along the X direction. The crack and crushing patterns are expressed in terms of the norm of the fracture and crushing strain tensor ($\mathbf{E}^f$ and $\mathbf{E}^c$, respectively), denoted as EFEQV and ECEQV. When the load acts in the positive direction of X, the Tower's connection with the surrounding building is characterised by significant fractures. Simultaneously, the Tower's base reaches the limit of compressive strength of the masonry, resulting in considerable crushing strain.

On the other hand, when the load is applied in the opposite direction, a crushing area develops in the connection area between the Tower and the building, at around 21 m high. On the opposite face, a horizontal fracture arises at approximately 23 m, which reaches the building-tower connection area at 21 m through the later walls, resulting in the mechanisms of composed overturning of the façade. This crack pattern follows a typical collapse mechanism found in masonry bell towers [25, 59] and sketched in Fig. 24c. Lastly, Fig. 24d shows a zoomed-in view of the crack pattern of the Tower, and also in this case, the numerical modelling can trace the collapse mechanism found in this element type [25, 59, 61], Fig. 24c).

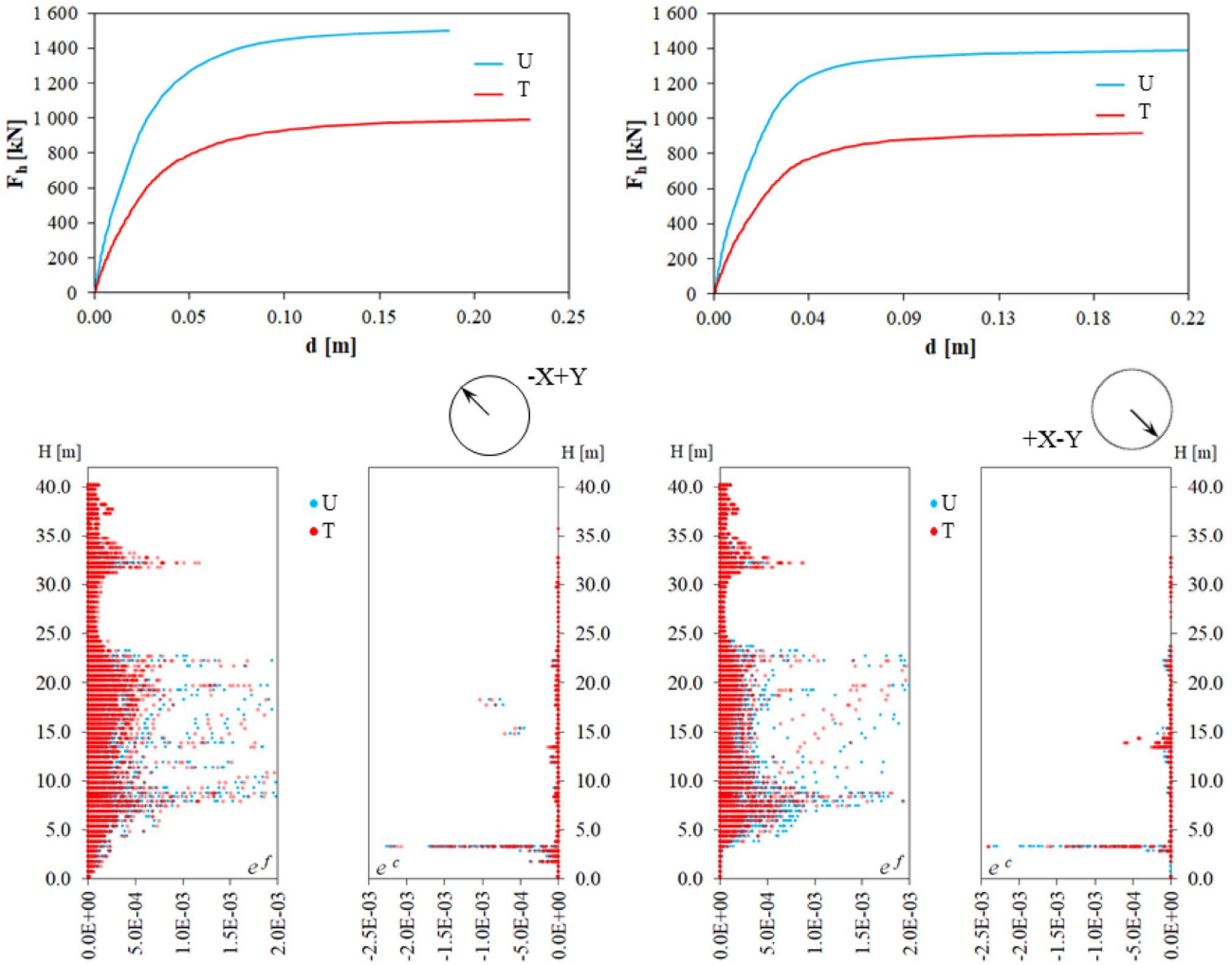

Fig. 22 Pushover analysis. Results for the load patterns U and T applied in the − X + Y and + X–Y directions: capacity curves (up); cracking and crushing distributions (bottom)

Assessments of the Tower's seismic capacity along the + X, + Y, and + X + Y directions have been carried out according to the N2 method [28]. Figure 25 shows the elastic response spectra (black lines) and the model's capacity curves (coloured lines) in the ADRS (Acceleration Displacement Response Spectra) format. The capacity curves have been obtained from the Tower pushover curves depicted in Figs. 19, 20, 21, according to Ref. [48]. The site demands of the area are traced considering a reference period of 75 years (black dashed line, SLD), 712 years (black continuous line, SLV) assuming a 50-year nominal life and a class coefficient equal to III [46]. The seismic demand has been assessed taking into account the seismic hazard in the Italian territory [60] and assuming a soil category C [47] evaluated by referring to the microzoning analyses described in Ref. [10]. The elastic spectra shown in Fig. 25a have been obtained taking a viscous damping of 1%, thus following the experimental results, while in (b) a 5% viscous damping is considered, according to the reference value reported in Ref. [47]. As already shown by the pushover curves, the structure exhibits the best performance along the Y direction for the U load distribution while lower performances are exhibited along the other two directions in terms of elastic stiffness, yielding and ultimate points. The figure also highlights the influence of viscous damping on the seismic vulnerability assessment.

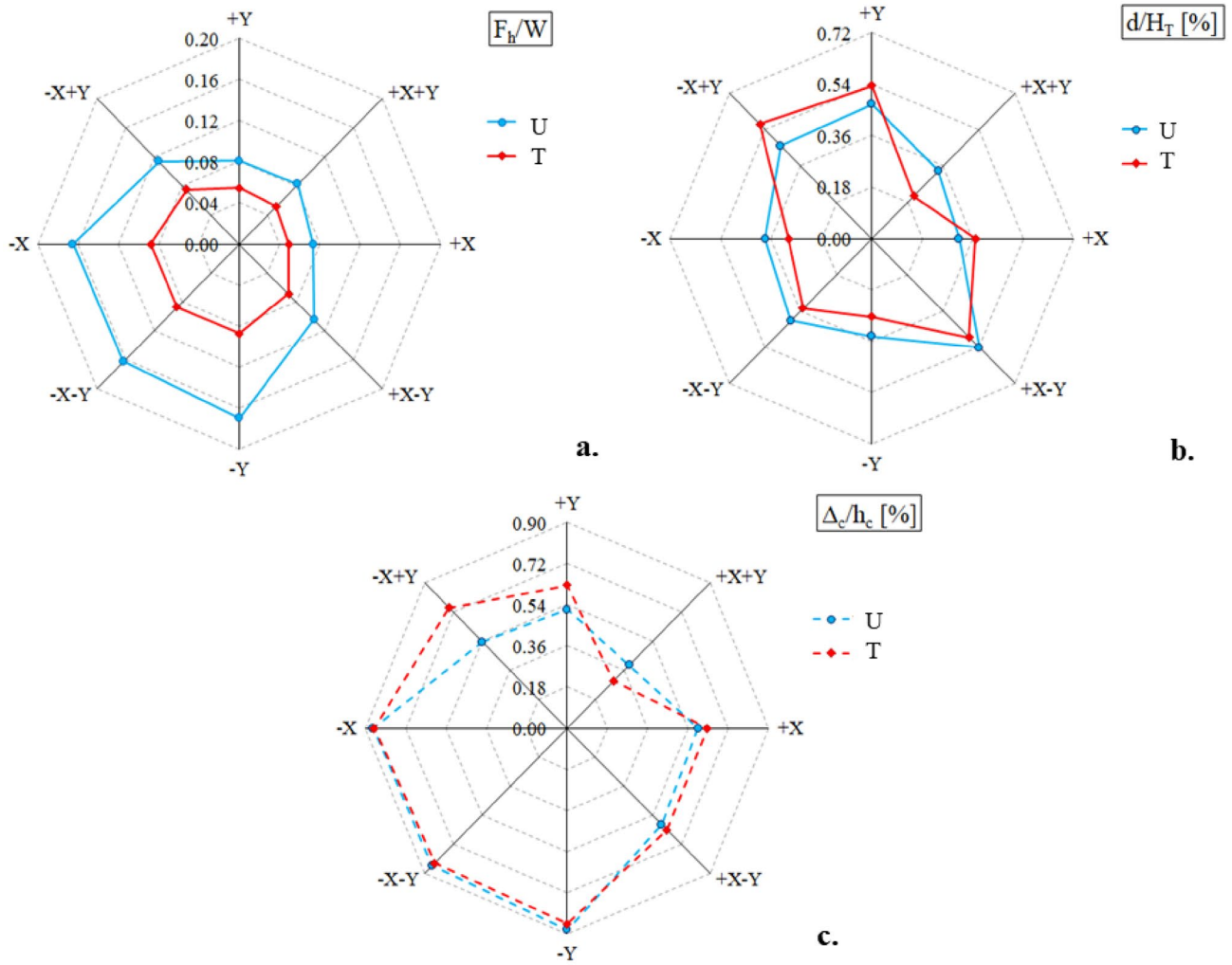

Fig. 23 Pushover analysis. Main results vs. direction of the applied loads: **a** collapse load F_h normalised to the Tower's self-weight W; **b** ratio (percentage) between d and the total height H_T of the Tower; **c** bell chamber's interstory drift (percentage)

4 Conclusions

The paper presents and discusses the results of the dynamic monitoring of the Tower of Palazzo dei Vicari inside the historic centre of Scarperia, a village exposed to high seismic hazards in the Mugello area. The Tower was the subject of three experimental campaigns. The first campaign was carried out from December 2019 to January 2020 on the occasion of the so-called Mugello seismic sequence, which featured an M 4.5 earthquake; the second and third dynamic tests were conducted in June 2021, in the absence of seismic excitation, and September 2023, when a seismic sequence struck the area near Scarperia. These tests aimed to characterise the Tower's dynamic behaviour under ambient and seismic excitations and check the response of the Tower over time. The experimental results were used to calibrate a FE model of the Tower and estimate the seismic vulnerability of the monument. To this aim, several numerical simulations were conducted on the calibrated model using the FE code NOSA-ITACA developed at ISTI-CNR for nonlinear structural analysis of masonry buildings. The dynamic behaviour of the Tower subjected to a seismic sequence recorded on 21 September 2023 by a seismic station at the base was investigated by comparing the velocities recorded along the Tower's height with their numerical counterparts. Furthermore, several pushover analyses were conducted to

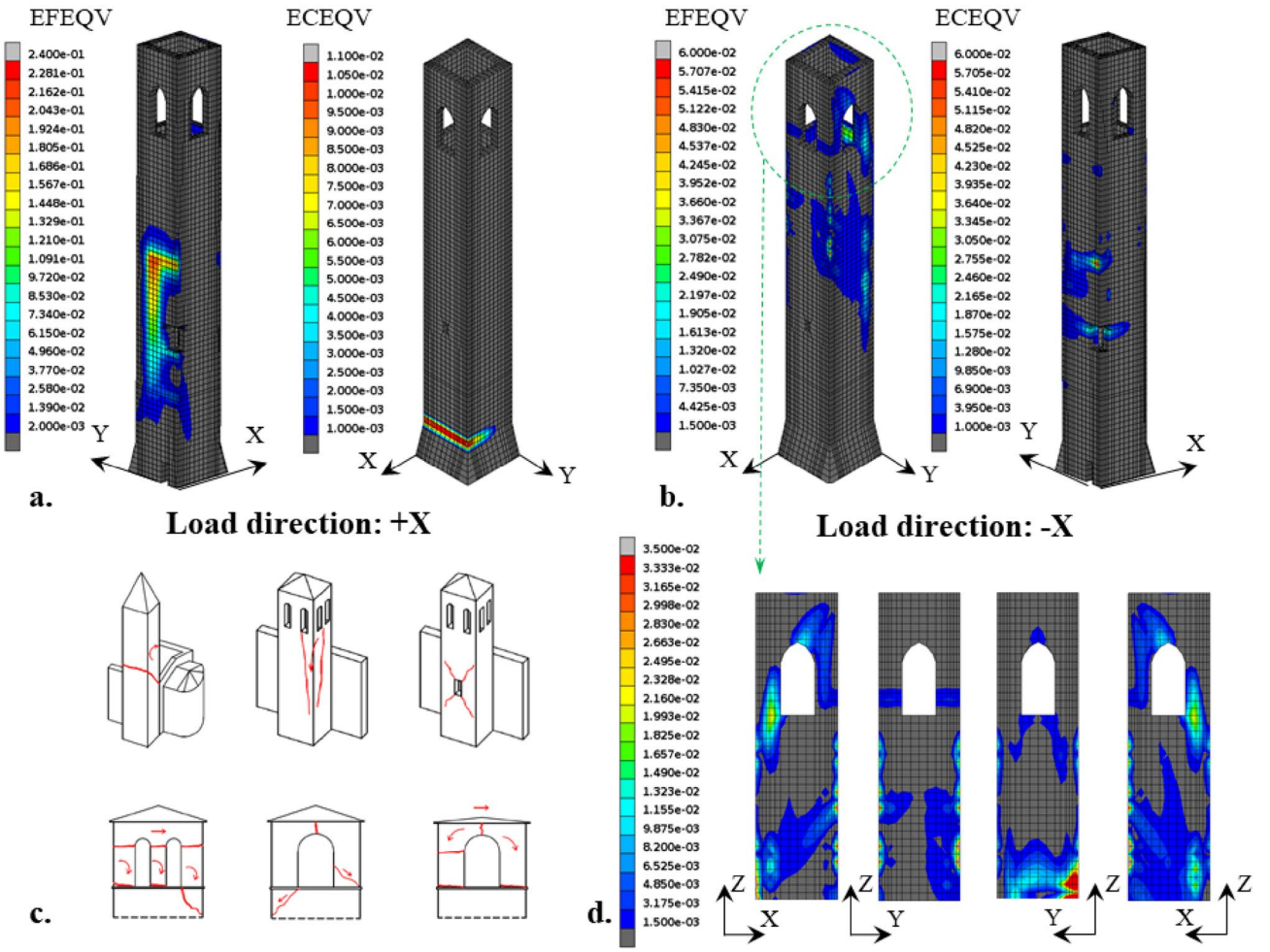

Fig. 24 Crack and crushing patterns result from load pattern T applied in the X direction (**a**, **b**); bell towers collapse mechanism reported in the literature (**c**); belfry fracture at the collapse (**d**)

investigate the collapse of the Tower as the load's distribution and direction varied.

The paper covers all the aspects of SHM, from data processing and dynamic identification to model updating and numerical simulation. Regarding the experimental campaign, the availability of records measured on a mediaeval tower over the years and during long seismic sequences is relatively uncommon and provides the opportunity to investigate the mechanical behaviour of the tower deeply. The software adopted for model updating and structural analyses is developed at ISTI-CNR and represents an original, non-commercial contribution to the numerical modelling of historical structure. The main outcomes of the experimental and numerical investigations can be summarised as follows:

- The wind, apart from the seismic events, is the most relevant vibration source recorded on the Tower during the experimental campaign. Comparing the diagrams of the wind speed, the seismogram recorded on the Tower and the temporal trend of the Tower's fundamental frequency, a clear correlation emerges between the energy content of the signal and the frequency values: in particular, the frequency decreases when the spectral amplitude and the energy content of the signal increase during the windiest days.
- Many seismic events have been recorded on the Tower during the experimental campaigns. Focusing on the most energetic event recorded, an M 3.1 earthquake, the Tower's dynamic behaviour remained substantially unchanged before and after the shaking. A frequency drop corresponding to the velocity and spectral amplitude peaks was observed during the seismic event.
- Dynamic identification of the Tower was performed after the three experimental campaigns from 2019 to 2023. Very similar values of the main Tower's frequencies were found in the three tests, thus proving substantial stability of the Tower's dynamic response in time.

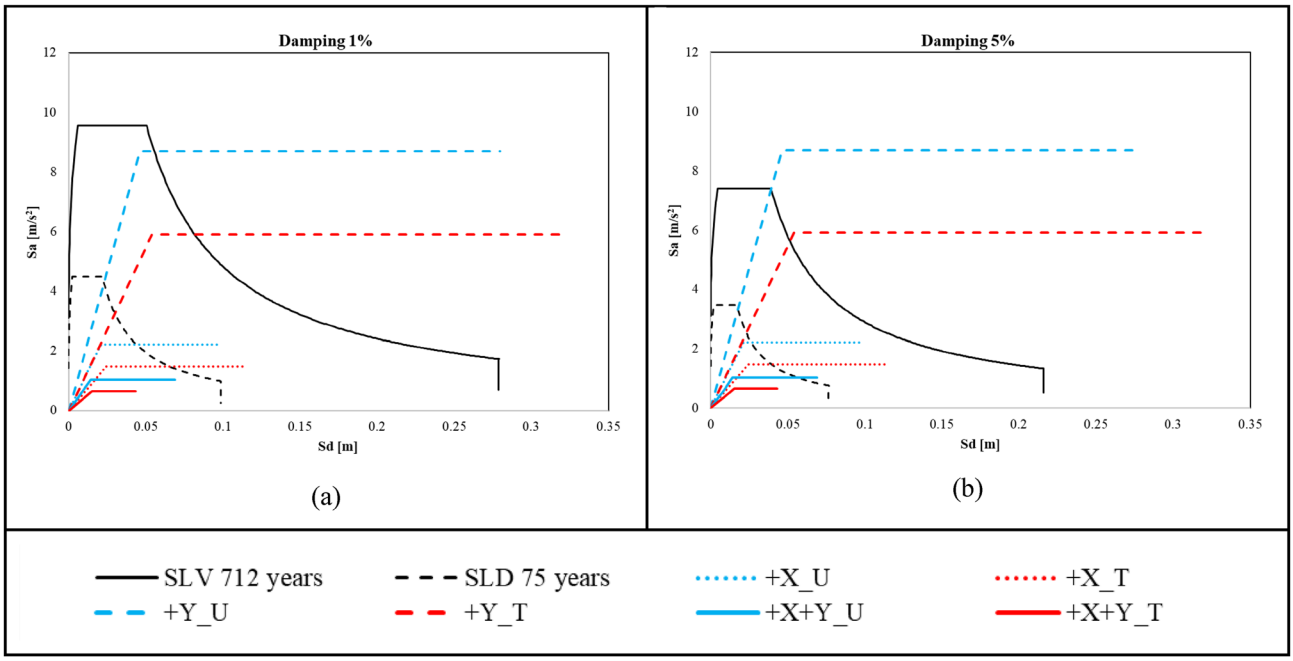

Fig. 25 Response spectrum and capacity curve in the ADRS format according to the different directions of analysis; **a** viscous damping 1%, **b** viscous damping 5%

- The experimental tests highlight low damping ratio values under 1%. This feature is evident when analysing the signals recorded on the Tower after the mainshocks and confirmed by the numerical simulation of the Tower's dynamic response under earthquake. A beating effect between the two main oscillations of the Tower has also been found, analogously to what was observed on similar slender masonry towers.
- Analysing the numerical and experimental responses to an M 2.6 seismic event recorded in 2023 provided a substantially good agreement between the model and the experimental responses.
- The pushover analyses conducted for different load distributions and directions allowed an assessment of the Tower's collapse load and crack and crushing distributions.

Acknowledgements This research has been partially supported by the Italian National Research Council (REVOLUTION Project, Progetti di Ricerca @CNR, 2022–2024). This support is gratefully acknowledged. The authors want to thank the mayor and the municipal administration of Scarperia e San Piero for their availability and support during the execution of the monitoring survey.

Funding Open access funding provided by ISTI - PISA within the CRUI-CARE Agreement.

Data availability The data that support the findings of this study are available upon reasonable request.

Declarations

Conflict of interest The authors declare that they have no conflict of interest.

References

1. Acito M, Chesi C, Milani G, Torri S (2016) Collapse analysis of the Clock and Fortified towers of Finale Emilia, Italy, after the 2012 Emilia Romagna seismic sequence: Lesson learned and reconstruction hypotheses. Constr Build Mater 115:193–213. https://doi.org/10.1016/j.conbuildmat.2016.03.220
2. Aloisio A, Antonacci E, Fragiacomo M, Alaggio R (2020) The recorded seismic response of the Santa Maria di Collemaggio basilica to low-intensity earthquakes. Int J Archit Herit. https://doi.org/10.1080/15583058.2020.1802533
3. Arrighetti A (2016) L'archeosismologia in architettura. Per un manuale, Firenze University Press, Firenze

4. Azzara RM, Cara F, Cultrera G, Di Giulio G (2004) Manuale d'uso dei programmi per lo scaricamento e l'analisi semi-automatica dei dati registrati da stazioni sismiche per lo studio degli effetti di sito. Rapporti tecnici INGV n. 25 2004, p 34
5. Azzara RM, Girardi M, Iafolla V, Padovani C, Pellegrini D (2020) Long-term dynamic monitoring of medieval masonry towers. Front Built Environ. https://doi.org/10.3389/fbuil.2020.00009
6. Azzara RM, De Roeck G, Girardi M, Padovani C, Pellegrini D, Reynders E (2018) The influence of environmental parameters on the dynamic behaviour of the San Frediano bell tower in Lucca. Eng Struct 156:175–187. https://doi.org/10.1016/j.engstruct.2017.10.045
7. Azzara RM, Girardi M, Padovani C, Pellegrini D (2023) Experimental investigations and numerical modelling: a fruitful interaction for the nonlinear dynamical analysis of masonry structures. Continuum Mech Thermodyn. https://doi.org/10.1007/s00161-023-01264-2
8. Azzara RM, Tanganelli M, Trovatelli F, Vettori N (2024) Results from the seismometric continuous monitoring of an ancient bell tower: The Arnolfo Tower, Palazzo Della Signoria, Florence, Italy. In: International Conference on Structural Analysis of Historical Constructions, vol. 47. Springer Nature Switzerland, Cham. pp 165–178 https://doi.org/10.1007/978-3-031-39603-8_14.
9. Azzara RM, Girardi M, Padovani C, Pellegrini D (2023) Dynamic behaviour of the carillon tower in Castel San Pietro Terme, Italy. Struct Control Health Monit 2023:1045234. https://doi.org/10.1155/2023/1045234
10. Baglione M, D'Intinosante V, Nencini V (2012) Microzonazione sismica, Relazione Illustrativa Comune di Scarperia, Attuazione dell'articolo 11 della legge 24 giugno 2009, n. 77, available at: https://www.regione.toscana.it/-/risultati-delle-indagini-nella-provincia-di-firenze
11. Baraccani S, Azzara RM, Palermo M, Gasparini G, Trombetti T (2020) Long-term seismometric monitoring of the Two Towers of Bologna (Italy): modal frequencies identification and effects due to traffic induced vibrations. Front Built Environ. https://doi.org/10.3389/fbuil.2020.00085
12. Barsocchi P, Bartoli G, Betti M, Girardi M, Mammolito S, Pellegrini D, Zini G (2021) Wireless sensor networks for continuous structural health monitoring of historic masonry towers. Int J Archit Herit 15(1):22–44. https://doi.org/10.1080/15583058.2020.171922
13. Bocciarelli M, Barbieri G (2017) A numerical procedure for the pushover analysis of masonry towers. Soil Dyn Earthq Eng 93:162–171. https://doi.org/10.1016/j.soildyn.2016.07.022
14. Boncio P, Brozzetti F, Lavecchia G (2000) Architecture and seismotectonics of a regional low-angle normal fault zone in Central Italy. Tectonics 19:1038–1055. https://doi.org/10.1029/2000TC900023
15. Brincker R, Ventura C (2015) Introduction to operational modal analysis. Wiley
16. Brunori Cianti L (2008) Palazzo dei Vicari a Scarperia, in Palazzo dei Vicari a Scarperia e Raccolta d'arte sacra "Don Corrado Paoli" a Sant'Agata, Bisceglia A, Brunori Cianti L (Eds) Edizioni Polistampa (in Italian)
17. Cardinali V, Cristofaro MT, Ferrini M, Nudo R, Paoletti B, Tanganelli M (2022) A multiscale approach for the seismic vulnerability assessment of historical centres in masonry building aggregates: cognitive approach and interdisciplinary perspectives. Int J Archit Herit 16(6):839–864. https://doi.org/10.1080/15583058.2021.1992536
18. Castello B, Selvaggi G, Chiarabba C, Amato A (2006) CSI Catalogo della sismicità italiana 1981–2002, versione 1.1. Istituto Nazionale di Geofisica e Vulcanologia (INGV). https://doi.org/10.13127/CSI.1.1.
19. Clinton JF, Bradford SC, Heaton TH, Favela J (2006) The observed wander of the natural frequencies in a structure. Bull Seismol Soc America 96(1):237–257. https://doi.org/10.1785/0120050052
20. Clough RW, Penzien K (1975) Dynamics of structures. McGraw-Hill, New York
21. Cole HA (1973) On-line failure detection and damping measurements of aerospace structures by Random Decrement Signature. NASA CR-2205
22. Cuadros-Rojas E, Saloustros S, Tarque N, Pelà L (2024) Photogrammetry-aided numerical seismic assessment of historical structures composed of adobe, stone and brick masonry: Application to the San Juan Bautista Church built on the Inca temple of Huaytará, Peru. Eng Fail Anal 15:107984. https://doi.org/10.1016/j.engfailanal.2024.107984
23. Degli Abbati S, Sivori D, Cattari S, Lagomarsino S (2023) Ambient vibrations-supported seismic assessment of the Saint Lawrence Cathedral's bell tower in Genoa, Italy. J Civ Struct Health Monit. https://doi.org/10.1007/s13349-023-00709-1
24. Di Giulio G, Vassallo M, Boscato G, Dal Cin A, Russo S (2014) Seismic monitoring by piezoelectric accelerometers of a damaged historical monument in downtown L'Aquila. Ann Geophys 57(6):S0654. https://doi.org/10.4401/ag-6671
25. Doglioni F, Petrini V, Moretti A (1994) Le chiese e il terremoto. Ed. LINT, Trieste (in Italian)
26. Dunand F (2005) Pertinence du bruit de fond sismique pour la caractérisation dynamique et l'aide au diagnostic sismique des structures de génie civil, Doctoral dissertation, Université Joseph-Fourier-Grenoble I
27. Ergün M, Tayfur B (2024) Evaluation of the seismic performance pre-and post-restoration of a masonry clock tower's FE model updated via experimental and optimization methods. Eng Fail Anal. https://doi.org/10.1016/j.engfailanal.2024.107986
28. Fajfar P (2000) A Nonlinear Analysis Method for Performance-Based Seismic Design. Earthq Spectra 16(3):573–592. https://doi.org/10.1193/1.1586128
29. Ferraioli M, Miccoli L, Abruzzese D (2018) Dynamic characterisation of a historic bell-tower using a sensitivity-based technique for model tuning. J Civ Struct Heal Monit 8:253–269. https://doi.org/10.1007/s13349-018-0272-9
30. García-Macías E, Ubertini F (2019) Seismic interferometry for earthquake-induced damage identification in historic masonry towers. Mech Syst Signal Process 132:380–404. https://doi.org/10.1016/j.ymssp.2019.06.037
31. Gentile C, Ruccolo A, Canali F (2019) Continuous monitoring of the Milan Cathedral: dynamic characteristics and vibration-based SHM. J Civ Struct Heal Monit 9(5):671–688. https://doi.org/10.1007/s13349-019-00361-8
32. Gentile C, Guidobaldi M, Saisi A (2016) One-year dynamic monitoring of a historic tower: damage detection under changing environment. Meccanica 51(11):2873–2889. https://doi.org/10.1007/s11012-016-0482-3
33. Girardi M, Padovani C, Pellegrini D, Robol L (2019) Nonlinear FE model updating for masonry constructions via linear perturbation and modal analysis. In: Papadrakakis, M. Fragiadakis (eds) COMPDYN 2019 7th ECCOMAS Thematic Conference on Computational Methods in Structural Dynamics and Earthquake Engineering M. Crete, Greece, 24–26 June 2019. https://doi.org/10.7712/120119.6992.18689
34. Girardi M, Padovani C, Pellegrini D, Porcelli M, Robol L (2023) Numerical modelling of historical masonry structures with the finite element code NOSA-ITACA. In: INdAM Workshop: Mathematical modeling and Analysis of degradation and restoration in Cultural Heritage. Springer Nature Singapore, Singapore. pp 133–152. https://doi.org/10.1007/978-981-99-3679-3_9.

35. Girardi M, Lucchesi M (2010) Free flexural vibrations of masonry beam-columns. J Mech Mater Struct 5(1):143–159. https://doi.org/10.2140/jomms.2010.5.143
36. Gueguen P, Michel C (2009) Time-frequency analysis of small frequency variations in civil engineering structures under weak and strong motion using reassignment methods. Struct Health Monit 9(2):159–171. https://doi.org/10.1177/1475921709352146
37. Guidoboni E, Ferrari G, Mariotti D, Comastri A, Tarabusi G, Sgattoni G, Valensise G (2018) CFTI5Med, Catalogo dei Forti Terremoti in Italia (461 a.C.-1997) e nell'area Mediterranea (760 a.C.-1500). Istituto Nazionale di Geofisica e Vulcanologia (INGV). https://doi.org/10.6092/ingv.it-cfti5
38. Locati M, Camassi R, Rovida A, Ercolani E, Bernardini F, Castelli V., Caracciolo CH, Tertulliani A, Rossi A, Azzaro R, D'Amico S, Antonucci A (2022) Database Macrosismico Italiano (DBM15), versione 4.0 . Istituto Nazionale di Geofisica e Vulcanologia (INGV). https://doi.org/10.13127/dbmi/dbmi15.4
39. Lucchesi M, Padovani C, Pasquinelli G, Zani N (2008) Masonry constructions: mechanical models and numerical applications: lecture notes in applied and computational mechanics. Springer, Berlin (**ISBN 978-354079110-2**)
40. Mantovani E (2005) Evolutionary reconstruction of the Mediterranean region: extrusion tectonics driven by plate convergence. In: Finetti IR (ed) CROP, deep seismic exploration of the Mediterranean region, vol 32. Elsevier, pp 705–746
41. Margheriti L, Nardi A, Mele FM, Marchetti A (2017) Bollettino Sismico Italiano, II quadrimestre 2016. Istituto Nazionale di Geofisica e Vulcanologia (INGV). https://doi.org/10.13127/BSI/201602
42. Margottini C, Ambraseys NN, Screpanti A (1993). La magnitudo dei terremoti italiani del XX secolo. ENEA, rapporto interno, Roma, 57
43. Masciotta MG, Ramos LF, Lourenço PB (2017) The importance of structural monitoring as a diagnosis and control tool in the restoration process of heritage structures: a case study in Portugal. J Cult Herit 17:36–47. https://doi.org/10.1016/j.culher.2017.04.003
44. Milani G, Clementi F (2021) Advanced seismic assessment of four masonry bell towers in Italy after operational modal analysis (OMA) identification. Int J Archit Herit 15(1):157–186
45. Mikael A, Gueguen P, Bard PY, Roux P, Langlais M (2013) The Analysis of Long-Term Frequency and Damping Wandering in Buildings Using the Random Decrement Technique. Bull Seismol Soc Am 103(1):236–246. https://doi.org/10.1785/0120120048
46. MIBACT (2011) Linee Guida per la Valutazione e Riduzione del Rischio Sismico del Patrimonio Culturale Allineate alle nuove Norme Tecniche per le Costruzioni (D.M. 14 Gennaio 2008) Rome
47. MIT (2018) Decreto 17 gennaio 2018 del Ministero delle Infrastrutture e dei Trasporti. Aggiornamento delle Norme tecniche per le costruzioni (in Italian)
48. MIT (2019) Circolare 21 gennaio 2019, n.7 C.S.LL.PP del Ministero delle Infrastrutture e dei Trasporti. Istruzioni per l'applicazione dell'Aggiornamento delle Norme Tecniche delle costruzioni di cui al decreto ministeriale 17 gennaio 2018 (in Italian)
49. Pianosi F, Sarrazin F, Wagener T (2015) A Matlab toolbox for global sensitivity analysis. Environ Model Softw 70:80–85. https://doi.org/10.1016/j.envsoft.2015.04.009
50. Pintucchi B, Zani N (2014) Effectiveness of nonlinear static procedures for slender masonry towers. Bull Earthq Eng 12:2531–2556. https://doi.org/10.1007/s10518-014-9595-z
51. Ponsi F, Bassoli E, Vincenzi L (2022) Bayesian and deterministic surrogate-assisted approaches for model updating of historical masonry towers. J Civ Struct Heal Monit 12(6):1469–1492. https://doi.org/10.1007/s13349-022-00594-0
52. Ramos LF, Marques L, Lourenço PB, De Roeck G, Campos-Costa A, Roque J (2010) Monitoring historical masonry structures with operational modal analysis: Two case studies. Mech Syst Signal Process 24(5):1291–1305. https://doi.org/10.1016/j.ymssp.2010.01.011
53. Reynders E, Schevenels M, De Roeck G (2014) MACEC 3.3: a Matlab toolbox for experimental and operational modal analysis. Department of Civil Engineering, KU Leuven. http://bwk.kuleuven.be/bwm/macec/
54. Rodrigues J, Brincker R (2005) Application of the random decrement technique in operational modal analysis. In: Proceedings of the 1st International Operational Modal Analysis Conference, April 26–27, 2005, Copenhagen, Denmark, ISBN 978-878160600-0
55. Romero-Sánchez E, Morales-Esteban A, Bento R, Navarro-Casas J (2023) Numerical modelling for the seismic assessment of complex masonry heritage buildings: the case study of the Giralda tower. Bull Earthq Eng 21:4669–4701. https://doi.org/10.1007/s10518-023-01714-x
56. Rossi A, Nardi A, Marchetti A, Mele FM, Margheriti L (2017) Bollettino Sismico Italiano, III quadrimestre 2016. Istituto Nazionale di Geofisica e Vulcanologia (INGV). https://doi.org/10.13127/BSI/201603
57. Rovida A, Locati M, Camassi R, Lolli B, Gasperini P, Antonucci A (2022) Italian Parametric Earthquake Catalogue (CPTI15), version 4.0. Istituto Nazionale di Geofisica e Vulcanologia (INGV), https://doi.org/10.13127/cpti/cpti15.4
58. Salachoris GP, Standoli G, Betti M, Milani G, Clementi F (2023) Evolutionary numerical model for cultural heritage structures via genetic algorithms: a case study in central Italy. Bull Earthq Eng. https://doi.org/10.1007/s10518-023-01615-z
59. Sepe V, Speranza E, Viskovic A (2008) A method for large-scale vulnerability assessment of historic towers. Struct Control Health Monit 15:389–415. https://doi.org/10.1002/stc.243
60. Stucchi M, Meletti C, Montaldo V, Akinci A, Faccioli E, Gasperini P, Malagnini L, Valensise G (2004) Pericolosità sismica di riferimento per il territorio nazionale MPS04 . Istituto Nazionale di Geofisica e Vulcanologia (INGV). https://doi.org/10.13127/sh/mps04/ag
61. Testa F, Barontini A, Chieffo N et al (2024) Observed damage and simplified risk assessment of Italian masonry bell towers struck by past seismic events. Bull Earthq Eng. https://doi.org/10.1007/s10518-024-01878-0
62. Ubertini F, Cavalagli N, Kita A, Comanducci G (2018) Assessment of a monumental masonry bell-tower after 2016 central Italy seismic sequence by long-term SHM. Bull Earthq Eng 16(2):775–801. https://doi.org/10.1007/s10518-017-0222-7
63. Valente M, Milani G (2016) Seismic assessment of historical masonry towers by means of simplified approaches and standard FEM. Constr Build Mater 108:74–104. https://doi.org/10.1016/j.conbuildmat.2016.01.025
64. Wathelet M, Chatelain JL, Cornou C, Di Giulio G, Guillier B, Ohrnberger M, Savvaidis A (2020) Geopsy: a user-friendly open-source tool set for ambient vibration processing. Seismol Res Lett. https://doi.org/10.1785/0220190360
65. Xu D, Xie Q, Hao W (2024) Seismic damage evaluation of historical masonry towers through numerical model. Bull Earthq Eng. https://doi.org/10.1007/s10518-024-01858-4